ABSTRACT

Small Molecule Inhibitors of Cruzain for Treatment of Chagas' Disease

Hijab Ahmed

Director: Mary Lynn Trawick, Ph.D.

Chagas' disease, a neglected tropical disease, affects millions worldwide. This zoonosis occurs as a result of parasitic invasion. The etiological organism, *Trypanosoma cruzi* (*T. cruzi*) enters mammalian host cells by triaatomine insects. There are two phases of the disease with different presented symptoms. Current treatment proves largely ineffective in the chronic phase and highly toxic, however no other treatment exists. Due to the treatments' negative side effects, there is an urgent unmet need for alternative treatments. A potential therapy lies in targeting cruzain, the recombinant form of cruzipain, because this cysteine protease is involved in nutrition, cellular remodeling, immune evasion, and parasitic replication throughout the life cycle of *T. cruzi*. Treatment of an infected mouse with the cruzain inhibitor K777 resulted in the eradication of the T. cruzi infection. This validates cruzain as a potential target for developing a curative treatment. A series of thiosemicarbazone derivatives synthesized by the Pinney laboratories as part of a collaborative project between the Trawick and Pinney laboratories at Baylor University were evaluated as inhibitors of cruzain. A plasmid for cruzain production by recombinant DNA was provided by the James McKerrow laboratory at UCSF. This study intended to evaluate these compounds as potential inhibitors of cruzain by ascertaining IC_{50} values against the enzyme. Moreover, advanced kinetic investigations of the most effective inhibitors were conducted so their mechanisms could be understood. Cruzain activity was monitored using a fluorogenic enzyme assay, which measured the concentration of 7-amino-4-methylcoumarin (AMC) product released from Z-FR-AMC, a synthetic substrate. A number of thiosemicarbazone compounds proved to be effective inhibitors of cruzain in the nanomolar range (29.5-312 nM). Progress curves and pre-incubation studies show these compounds as time-dependent inhibitors. Several cruzain inhibitors evaluated in these studies should advance as potential therapeutic agents for Chagas' disease.

APPROVED BY DIRECTOR OF HONORS THESIS:

_____

Dr. Mary Lynn Trawick

Department of Chemistry and Biochemistry

APPROVED BY THE HONORS PROGRAM:

_____

Dr. Elizabeth Corey, Director

DATE: _____

SMALL MOLECULE INHIBITORS OF CRUZAIN FOR TREATMENT OF CHAGAS' DISEASE

A Thesis Submitted to the Faculty of

Baylor University

In Partial Fulfillment of the Requirements of the

Honors Program

By

Hijab Ahmed

Waco, Texas

May 2016

TABLE OF CONTENTS

LIST OF FIGURES

LIST OF TABLES

LIST OF EQUATIONS

LIST OF ABBREVIATIONS

NF	Nifurtimox
BZN	Benznidazole
IC_{50}	inhibitory concentration which reduces maximal reaction velocity by 50%
TSC	thiosemicarbazone
Z-FR-AMC	benzyloxycarbonyl-L-phenylalaninyl-L-argininyl-7-amino-4-methylcoumarin
DMSO	dimethyl sulfoxide
DTT	dithiothreitol
NaOAc	sodium acetate
EDTA	ethylenediaminetetraacetic acid
AMC	aminomethylcoumarin
RPM	revolutions per minute
RFU	relative fluorescence units
SE	standard error

ACKNOWLEDGMENTS

First, and foremost, I would like to thank Allah (SWT) for creating this opportunity for me. I would like to acknowledge Dr. Mary Lynn Trawick, my thesis director, for her patience, kindness, time, and mentorship. I was privileged to have a mentor who gave so much of her time to me especially during early mornings, late nights, and even weekends. She has worked patiently with me as I worked on this project. Secondly, I would like to thank Dr. Kevin Pinney and former members of his lab, Drs. Erica Parker and Lindsay Jones for synthesizing the compounds evaluated in this study. I would like to thank Dr. McKerrow at UCSF for providing *T.* cruzi DNA used to synthesize cruzain. In addition, I would like to thank Dr. Michelle Nemec, the director of Molecular Bioscience Center, for facility use. Also, thanks to Baylor University for the opportunity to conduct research. I would like to thank Samuel Odutola, a graduate student who served as my lab mentor, for his patience. I am not sure how many times I asked him to explain a concept to me, but each time he did so without condescension. It is very rare to find this kind of warm patience, and I am so grateful I found this. I always felt like I could ask him any question. I also greatly appreciate his help in other matters like my analytical and organic chemistry classes. I want to thank Dr. Tracy Strecker for all the puns, jokes, and plain hilarity he offered. He always had a smart, hilarious remark regardless of the situation. I appreciated this humor especially in face of grueling data analysis. In addition, I want to thank Emily Taylor, for her compassionate and caring attention in my final year of

research. She just entered the lab, but gave me her time and counsel anyways. I have learned a lot from her, inside and outside the lab. Thanks also to Prashant Appitakala, Chioma Ikedionwu, Dr. Jeff Schwartze, and Yifan for their companionship and support. Finally, I would like to thank my committee members, Drs. Amanda Sevcik and Erika Abel for their forgiving patience and time as I prepared for my oral defense.

CHAPTER ONE

Introduction

This chapter will present a review of the current literature on Chagas' disease, alternative targets for therapeutic development with a special emphasis on cruzain and its inhibitors.

Introduction to Chagas disease

Chagas' disease, or American trypanosomiasis, caused by the parasitic protozoan, *Trypanosoma cruzi* (*T.cruzi*), poses a significant public health crisis in the western world. It has been identified as one of the five neglected parasitic infections by the United States Center for Disease Control, due to the worldwide volume and severity of infection, exacerbated by poor clinical management and stage dependent detection. [1]

Primary transmission occurs via triatominae, a family of blood sucking insects, commonly referred to as the "kissing bug". The fecal remains left at the bite contain the protozoan, which subsequently enters the bloodstream through the wound. Once blood borne, T. cruzi persists indefinitely in circulation, at which it may be secondarily distributed medically, by or donation or umbilical cord blood, for example.[2–4] Despite rigorous efforts in Latin America to limit primary outbreak, Chagas' disease remains endemic, with at least 300,000 and 80,000 projected cases in the United States and Europe, respectively, due to population migration. [1,4–6] Increased geographic distribution from Mexico to Canada, as illustrated in Figure 1, shows the severity of Chagas' disease

spread.[7] The mounting threat of advancing geographical expanse motivates development of curative, cost-effective pharmacological agents against this disease.

Figure 1. Projected number of *T. cruzi* infections in North America[7]

Life cycle of T. cruzi and transmission of T. cruzi

Upon infection, trypanosomes undergo environmentally stimulated morphological and biochemical stages, oscillating between trypomastigote and amastigote, illustrated in Figure 2. In the bloodstream, a trypomastigote initiates entry into the cell by stimulating recruitment of lysosomes to the plasma membrane. At fusion of the lysosome, the parasite enters the acidic compartment, which incites secretion of Tc-Tox, a proteolytic peptide, further lowering the pH, stimulating the transformation to the latent amastigote.

To reenter the circulation and complete infection, amastigotes revert back to the trypomastigote and elicit lysis.[8,9]

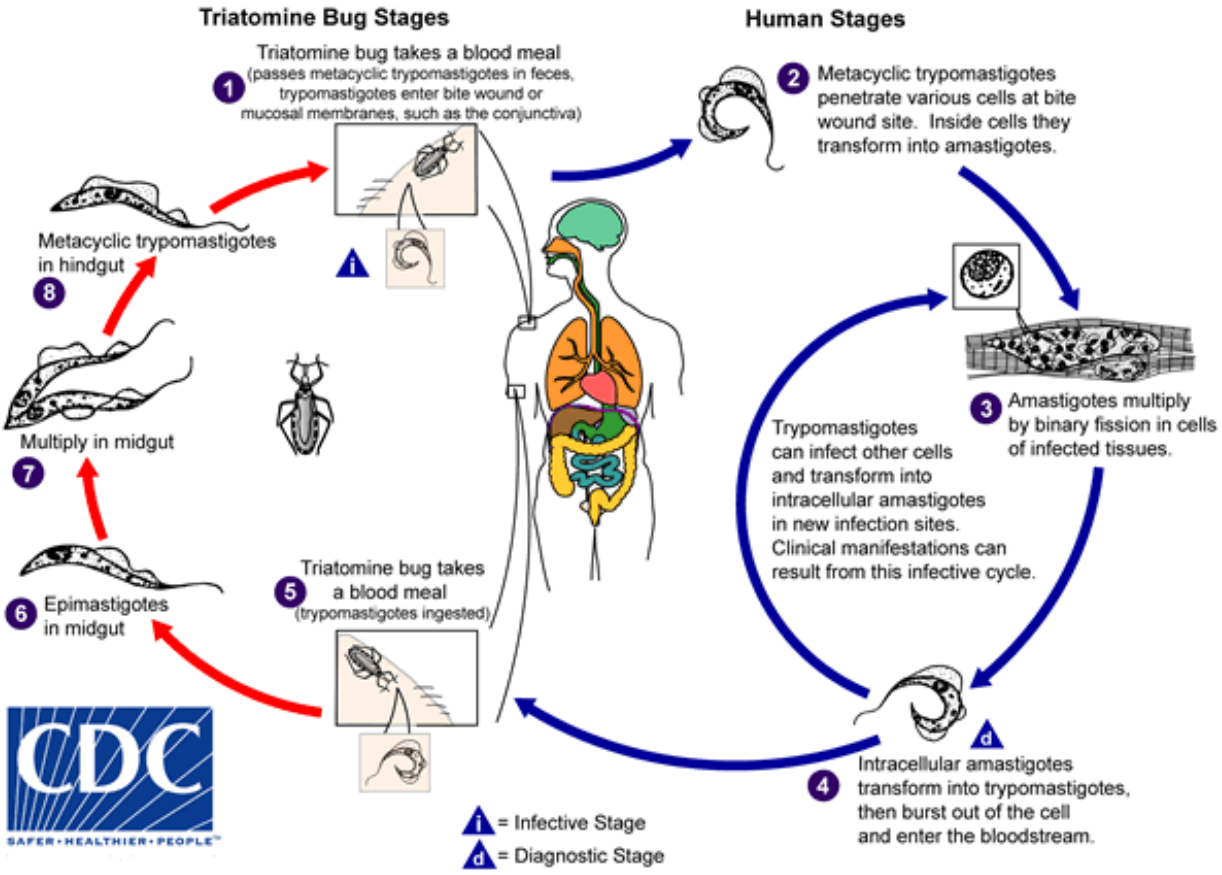

Figure 2. Life cycle and transmission of *T. cruzi*[10]

Pathology of Chagas' disease

If left undiagnosed, Chagas' disease is clinically manifested in two distinct phases-acute and chronic. The acute phase classically presents fever, enlarged liver and spleen, malaise, and facial edema, typically lasting from 8 to 12 weeks. In extreme cases, lethally dilated myocardiopathy has been observed. Beyond the initial symptomatic onset, disease enters a dormant period, referred to as the indeterminate form, lasting up to 30

years. Prolonged infection irreparably damages cardiovascular tissues leading to a wide variety of comorbid complications.[11] The chronic form presents as idiopathic cardiomyopathy. [5,12,13]

Current treatment of Chagas' disease

Currently there are two types of treatments: antiparasitic and symptomatic treatment. The former results in parasitic death and is effective in the acute phase while the latter is mainly palliative and is used for the chronic phase. Available drugs for the acute phase are nifurtimox (NF) and benznidazole (BZN). These nitroheterocyclics, as illustrated in Figure 6, interfere with the organism's genetic synthetic processes and create radicals allowing for antitrypanosomal activity.[14] Unfortunately, radicals harm the host as well resulting in undesirable immediate and lasting side effects such as neuropathy and cancer.[14,15] While antiparasitic therapy addresses acute stages, at the present time, no curative treatment is established for chronic Chagas' disease, when it is least detectable. Due to deleterious side effects, BZN is banned in some countries like United States. In absence of alternative treatment, BZN is still used in other countries especially in light of its use in the chronic form.[13,16] In particular, a newly created pediatric form, is used in such countries. As a result of the undesirable current treatment, there is a great unmet need for design of alternative therapeutics.

Drug targets

There are different potential targets including sterol and isoprenoid biosynthesis like C14a-demthylase (CYP51), transport pathways, cysteine protease cruzipain, redox systems, polyamine metabolism, and trypanothione synthesis. [17,18] Promising CYP51 inhibitors like posacazonole were recently evaluated in CHAGASAZOL clinical trial.

Unfortunately, these were associated with treatment failure after 10 months.[16] Another CYP51 inhibitor, currently in clinical trials as an antifungal drug, also shows promise as a curative agent for Chagas' disease.[19] In addition, VN1, another CYP51 inhibitor, showed 100% cure rate and survival in both murine models of acute and chronic forms.[20] However, the focus of this research is on cysteine proteases, specifically cruzipain since enzyme inhibition in a murine model of acute *T. cruzi* infection demonstrated curative effects.[21]

Cruzipain

Cruzipain is a lysosomal cysteine protease, a papain-like enzyme belonging to Clan 1A family. It is also a cathepsin-L and cathepsin-S like molecule which means inhibitors of cathepsin L and S have been shown as likely inhibitors of cruzain, the recombinant form of cruzipian. Mutations of cathepsin S show cruzain-specific activities when a Glu is introduced at position 205.[17] It can also be described as a cathepsin-F like molecule. It shares 50.5% sequence identity with cathepsin F. Cruzain, the recombinant form of cruzipain, lacks the C-terminal domain. Architecture includes a pro-region that can serve as a chaperone, as a potent inhibitor of enzymatic activity, and as an important molecule for trafficking within the cell. As shown in Figure 3, the structure of this enzyme is a folded single polypeptide chain with two separate domains connected by a polythreonine-rich area. The primary sequence contains a catalytic domain that harbors 205 amino acids. Of important significance, there is His162, Cys25, Asn182, and Asn21. Also, the catalytic triad involves Cys25, His159, and Asp175. This enzyme is heavily N-

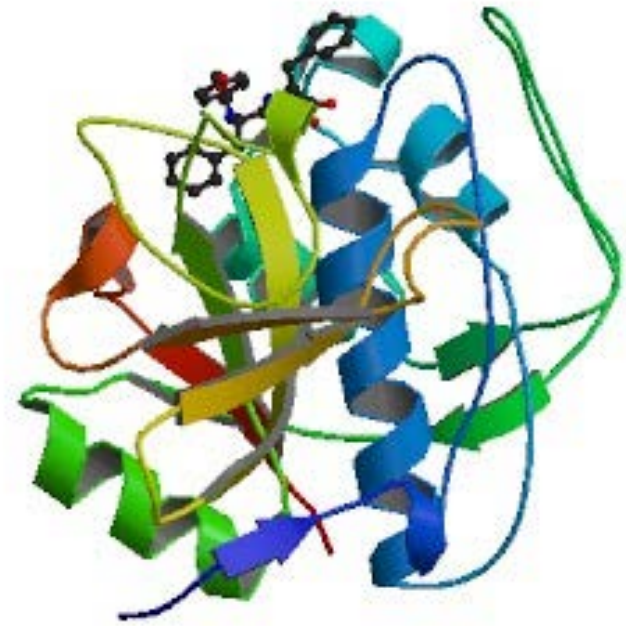

Figure 3. Crystal structure of cruzain[57]

and O-glycosylated as well as possibly sialycilations in the C-terminal domain. [17,21–23] The enzyme contains a deep, hydrophobic S2 pocket specifically due to the amino acid at the base of this pocket, Glu205. This can accommodate an arginine residue at the P2 position on the substrate. It can also accommodate Leu, Phe, Tyr, Val, Trp, and Ile in that order. [17] As shown in Figure 4, there are eight binding sites for the substrate labeled as S1,S2, S3, S4, S1',S2',S3', and S4'. These bind to respective peptide amino acids labeled accordingly where P is used instead of S. [24] The specificity pocket in addition to the catalytic triad and oxyanion hole allow for inhibition. The active site of the protease binds to the peptidic substrate through interactions between backbone and side chains. [25]

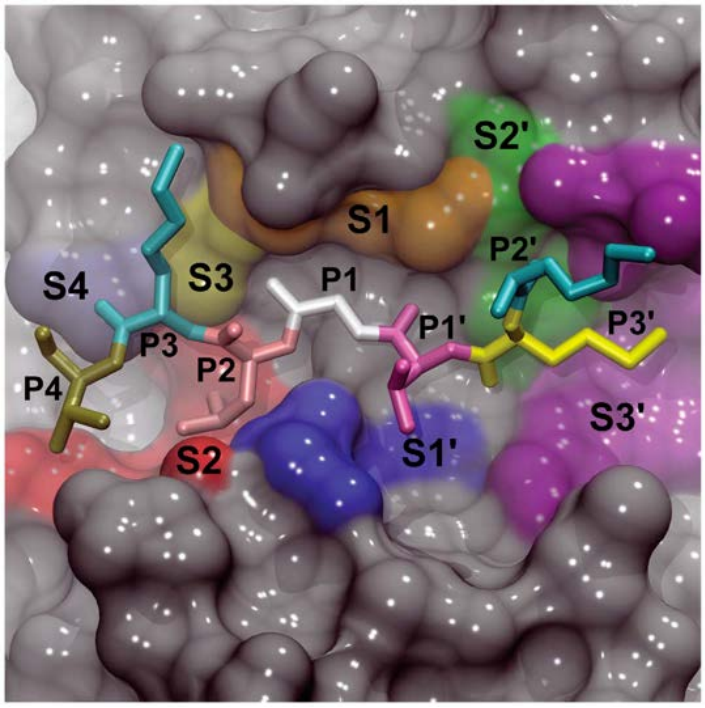

Figure 4. Active site of cruzain[24]

Cruzain is derived from a whole host of paralogous genes that explain its complex heterogeneity. There are 37-130 copies depending on which strain and which stage the organism is in. This makes therapies from a genetic standpoint like vaccines challenging.[17]

This cysteine protease plays an important role in parasitic development. It is present in varying concentrations throughout the life cycle of *T. cruzi* where it is in higher concentrations in the amastigote form within the human and the epimastigote form within the insect. It is involved in metacyclogenesis, host cell invasion, cell-remodeling, nutrition, and immune evasion.[26,27] In particular, it proteolytically cleaves the macrophage nuclear factor NF-KB P65. Cruzain also releases kinin in order to activate bradykinin receptors. Consequently, trypomastigotes exit the host cell's cytoplasm for further infection of the mammalian host. [17]

General mechanism of action of cruzipain

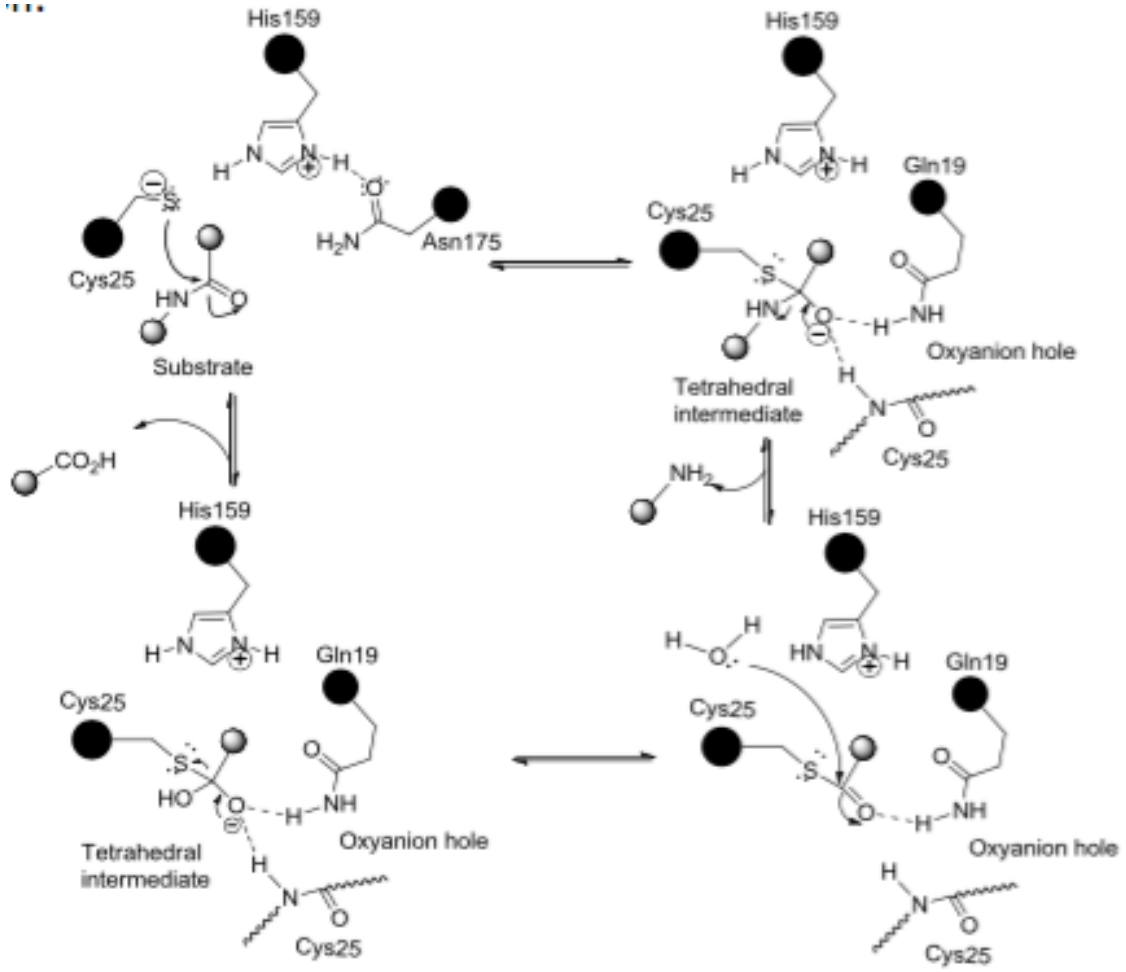

Figure 5. General mechanism of action for cruzipain[28]

As illustrated in Figure 5, the general mechanism of action involves a nucleophilic attack of the thiolate anion of the catalytic cysteine residue. Inhibitors are generally designed in order to affect enzymatic catalysis.

In the event of inhibition, unprocessed cruzipain accumulates in the Golgi apparatus. This accumulation interferes with the secretory pathway which eventually leads to trypanocidal activity.[17] Inhibition of cruzain, a recombinatory form, in a murine

model demonstrated curative characteristics validating cruzain as a target for therapeutic development. For design of effective inhibitors, compound must be i) orally effective in both stages, ii) completed under 60 days for clinical use, iii) of low molecular weight, iv) highly selective, v) highly bioavailable orally, vi) marginally toxic, vii) tolerated well, and viii) have negligible side effects.[28] This thesis summarizes the identification of potent cruzain inhibitors *in vitro*.

Cruzain inhibitors

Identification of potent cruzain inhibitors are done through substrate library screening, docking campaigns, high-throughput screening (HTS), virtual screening (VS), and quantitative structure-activity relationships (QSAR) established with x-ray crystallography and protein-ligand interactions fingerprint (PLIF) method. It is also clear that combining some of these methods identify chemotypes that were excluded upon using only one method. Combinatorial chemistry refers to the specific use of synthetic chemistry for the production of large number of substances. HTS refers to the analysis of large quantities of compounds as potential reacting agents in certain chemical reactions using computers, robots, liquid-handling devices, and sensitive detectors. VS or docking-based VS refers to a computer model of molecules fitting into the active site using advanced algorithms consequently ranking molecules as potential leads. In order to eliminate compounds incompatible with human physiology, crystal structures of ligand bound to cruzain are obtained by x-ray crystallography as illustrated in Figure 3.

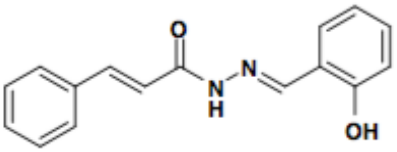

Cinnamic-N-Hydrazone

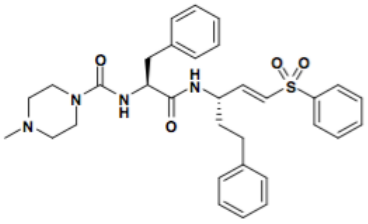

K777

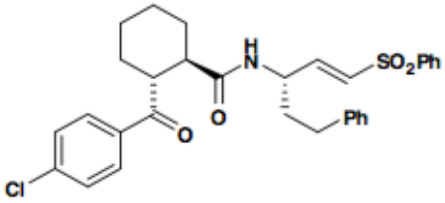

Vinyl sulfone derivatives

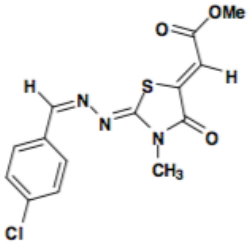

Thiazolidinones

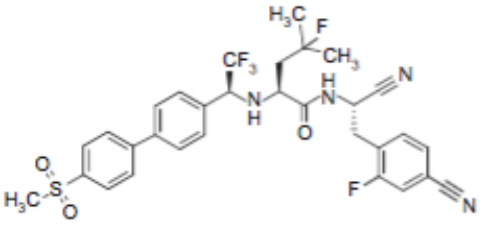

Cz007

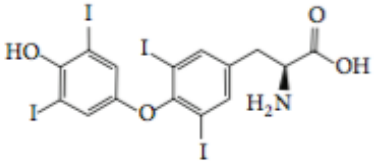

Levoxythroxine

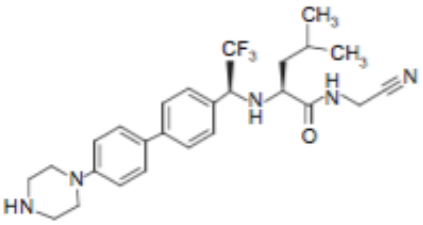

Cz008

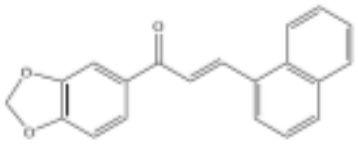

Chalcones

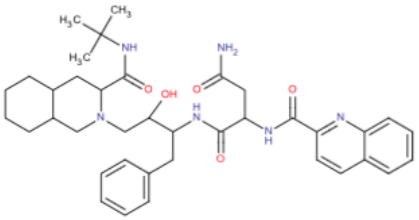

Saquinavir

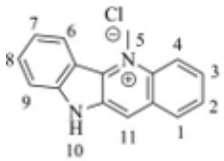

Cryptolepine (**1**)

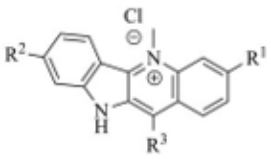

Cryptolepine Analogues (**2**)

R^1, R^2 = H or Cl

R^3 = Alkyl, cycloalkyl or aryldiamine

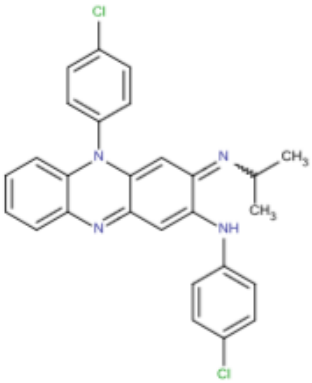

Clofazimine

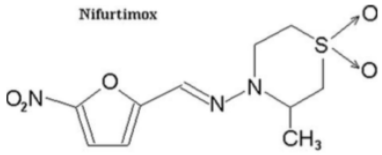

Nifurtimox

Benznidazole

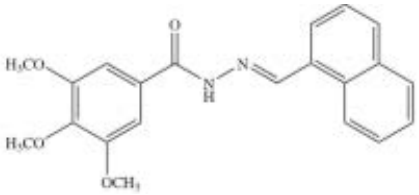

Hydrazide derivative

Figure 6.Structural representations of several compounds that inhibit cruzain[15,17,29–35]

Ferreira et al. identifies five new chemotypes through combined efforts of HTS and docking studies.[36] Based on screening methods and experimental findings, a host of cruzain inhibitors exist. Inhibitors differ primarily based on the type of warhead present. Examples include TSCs, vinylsulfones, derivatives of vinylsulfones, thiazolyl hydrazones, some of which have been added as a moiety to TSC compounds, alkklydiamine cryptolepine derivatives, compounds containing the 2-acetmidothiophene-3-carboxamide class, natural inhibitors like chagasin or tigutcystatin, repurposed drugs. Representative structures bearing respective warheads are illustrated in Figure 6. The characteristics of inhibition along with clinical data, if available, will be discussed below.

Reevaluating drugs for alternative purposes indicated potential use for cruzain inhibition. Such drugs, depicted in Figure 6, demonstrate micromolar affinity. For example, Bellera et al. identified the approved drugs Clofazimine, benidipine, and saquinavir as potential antichagasic candidates. However, clofazimine demonstrated excellent candidacy due to high tolerability, reversibility, reduced parasitemia load in a canine model of acute *T.cruzi* infection, and dosage similarity with current use of drug. Although the canine model did not result in complete cellular eradication, the concentration administered was five times less than administered dosage of BZN.[35] In addition, levoxythroxine, normally used for hormone replacement therapy, demonstrated cruzain inhibition with an IC_{50} value of 38.43±6.82 μM.[31] It is clear that repurposing drugs is a promising area for antichagasic candidates.

Other cruzain inhibitors include natural products such as chagasin and tigutcystatin. Chagasin is another natural, but ineffective cruzain inhibitor. [37] Tigutcystatin is derived from a vector of *T. cruzi*, traiatoma infestans, an insect. This

endogenous inhibitor was first shown to tightly and reversibly bind toward cruzipain (K_i=3.29 nM). Structural features of this particular cystatin involves a highly conserved N-terminal glycine residue, a principal motif (QxVxG where x refers to any amino acid residue), and two adjacent residues at the carboxyl end-proline and tryptophan. It is important to note these features are particularly significant to the general mechanism of cysteine protease inhibition. A type 2 cystatin, function of tigutcystatin remains largely unknown, however the same study that first demonstrated cruzain inhibition attempted to investigate the biological mechanisms in triaatomine insects. Possible physiological processes involving tigutcystatin include endogenous gastrointestinal cysteine proteases monitoring, inhibition of cruzain upon *T. cruzi* infection, and other innate immune mechanisms. [38] However, it is clear that this innate immunity is not sufficient to thwart *T. cruzi* pathogenesis. Therefore, natural inhibitors are lacking in terms of potential treatment options.

Metal-based cruzain inhibitors are compounds coordinated with metal ions, specifically platinum. Pt(II) complex has been shown to interact with thiol groups and possess inhibition of parasite growth. It is suggested that upon binding to the cysteine protease, free radicals are generated and DNA is intercalated.[39]

Derivatives of cryptolepine, an indoloquinoline alkaloid, exhibit cruzain inhibitory properties. Both crypotelepine and derivatives are shown in Figure 6. In one study, a secondary amine nitrogen atom at the piperidine moiety was shown to form a hydrogen bond with the amide carbonyl oxygen atom of Asp161. This nitrogen atom is also suggested to form an electrostatic interaction with the carboxylate group of the same residue. In this same study, derivatives with acyclic aminoalkylamine side chains are

shown to occupy both S1' and S2 subsites while others with less flexible side chains occupy only the S1' subsite. These compounds are potent agents due to the low cytotoxicity profiles and increased selectivity for the parasite.

Peptidyl drugs refer to a specific set of cruzain inhibitors, however, due to their low oral bioavailability, these drugs are not as promising as non-peptidic drugs. Although these drugs do not stand as efficacious inhibitors, the vinyl sulfone compound K777, as shown in Figure 6, served as "proof-of-concept" for cruzain inhibition as previously mentioned. Structural variants of irreversible K777, specifically at P1, P2, and P3 sites, showed that a hydrophilic heterocycle at P3 site favored hydrogen bonding with Ser61 of S3 subpocket. Other peptidyl compounds such as aldehyde-based and ketone-based inhibitors demonstrate picomolar inhibition.[40] General modifications of a ketoamide, as seen in Figure 6, produced reversible transition state analogs as suggested by kinetic studies, molecular modeling, and crystal structure. [40]

Other non-peptidyl drugs such as nitrile derivatives serve as competitive, reversible cruzain inhibitors. Examples of certain nitrile compounds are shown in Figure 6. In particular, amino nitriles have exhibited low nanomolar inhibition of cruzain. Further optimization around three different portions of the compound, P1, P2, and P3, resulted in specific SAR. For example, inhibitor potency dramatically increased with the presence of a F-like residue in P1 while hetorocyclic nitrile analogs did not affect potency. In addition, compounds bearing the S configuration proved significant for P1 in terms of potency. However, structural modifications of P1 or P3 did not result in enhanced selectivity. Although these areas did not pan out in terms of selectivity enhancement, differences in P2 site enhanced selectivity validating this area for further

enhancement. Mechanism of inhibition for amino nitrile compounds involves the nitrile warheard forming a reversible thiomidate with the catalytic cysteine residue of inhibitor.[41] Other nitrile inhibitors include Cz008 and Cz009 as depicted in Figure 6. These compounds demonstrated high selectivity where the most potent compound had an IC_{50} value of 1 nM. Furthermore, animal model studies with compound Cz008 showed 78% cure rate at 3 mg/kg. As indicated by its structure, Cz008 is a basic compound which allows for inhibition of extracellular cruzipain as a result of accumulation of the basic compound in the lysosome.[32] Basic inhibitors are problematic since these do not distinguish between host cathepsins and cruzipain. From Cz008 and Cz009, other nitrile based inhibitors with structural alterations at P1, P2, and P3 sites were developed in order to ascertain the binding mode of these particular inhibitors. Reversibility of compounds was established by monitoring the recovery of cruzain activity following a large, rapid dilution of enzyme-inhibitor complex. Molecular modeling suggests covalent bonding.[42] Molecular modeling of the most potent compound in this study is shown in Figure 7.

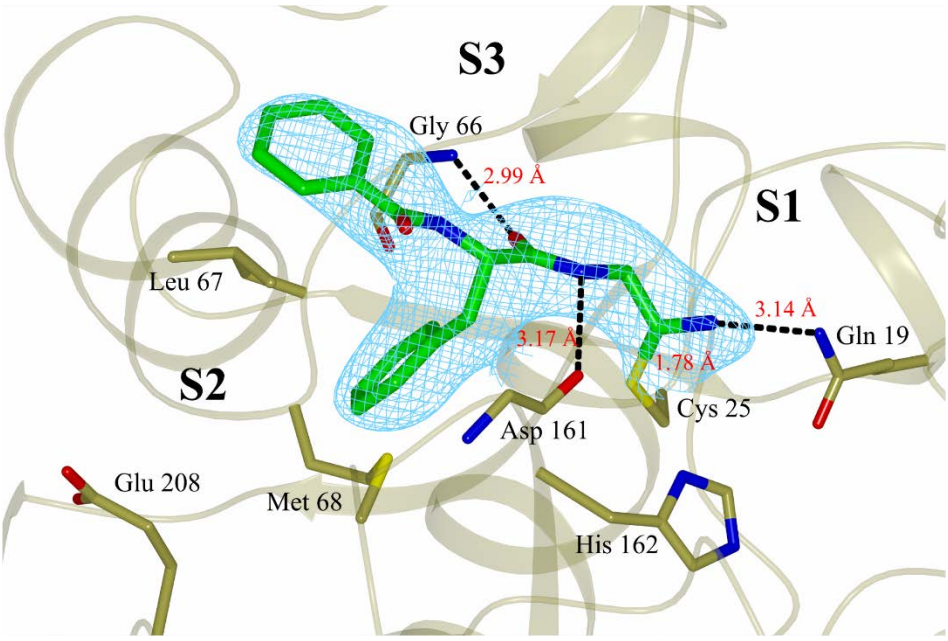

Figure 7.Molecular modeling of dipeptidyl nitrile with active site of cruzain[42]

Compounds with substituted phenylalanine showed deep penetration into the S2 pocket, a large hydrophobic region. Interestingly, these cruzain inhibitors showed poor antitrypanosomal activity, specifically against Tulahuen and Cl-Bren *T. cruzi* amastigote strains. [42] This suggests another mechanism of inhibition other than cruzain.

Chalcone and hydrazide derivatives inhibit cruzain in the low micromolar range. Chalcone analogs were synthesized via an aldol condensation of aryl aldehydes with acetophenone. Most of the potent chalcone analogs bore the methylenedioxyphenyl moiety suggesting a structural contribution to inhibition. Unfortunately, hydrazide derivatives demonstrated moderate cruzain inhibition compared to chalcones.[33] Chalcones are irreversible inhibitors that act as Michael acceptors by forming a covalent bond with the cysteine residue located in the active site. [30] While chalcones are more potent than hydrazides, these compounds are not as desirable as other nanomolar inhibitors.

Interestingly, acylhydrazides are structurally related to chalcones. Likewise, these compounds are used to form acylhydrazones representing a different core structure for cruzain inhibition. Cinnamic-N-acylhydrazone compounds were designed in such a manner to allow for a nucleophilic attack of the cysteine residue on either of two electrophilic sites. Interestingly enough, this study demonstrated the poor cruzain inhibitory properties in contrast to the excellent antitrypanosomal activity. The best inhibitors had IC_{50} values as low as 44.7 μM.[30] Therefore, there is another mechanism of action other than cruzain inhibition.

Thiazolylyhydrazones, structurally related to TSCs, represent another set of cruzain inhibitors. Aryl-4-oxothioazolylyhydrazones were shown to be effective cruzain inhbitiors where the most potent compound has an IC_{50} value of 0.3 μM. Analogues indicated that lengthening the linker between the heterocycle and the aromatic ring results in decreased potency. Also, this work showed that p-bromo substitution is far more potent with a *p*-chloro substitution. Furthermore, it was shown that conversion of the thioamide amino group to 4-thiazolidone ring resulted in increased activity. The mechanism of action for thiazolylyhydrazones can be understood from molecular modeling. Molecular modeling of aryl-4-oxothioazolylhydrazones indicate these compounds constructs hydrophobic and polar interactions with cruzain. In particular, the Asp158 forms crucial hydrogen bonds between the enzyme and the most active compound.[43]

Further modification of the thiazolinic ring results in cruzain inhibitors such as 2-iminothiazolidin-4-one, better cruzain inhibitors when compared to structural variants of thiazolidinones. These compounds with a thiocarbonyl, similar to TSCs, exhibit greater

potency than compound without the thiocarbonyl. Furthermore, the thazolidinic ring was proven crucial for inhibitory processes due to the binding sites' electronic- and stereospecificity.

TSCs represent another warhead evaluated as potential antichagasic compounds. Du et al. validated the TSC as cruzain inhibitors by enzymatic assays. Initially, these compounds were screened for inhibition of cathepsin L as part of a search for anticancer drugs in Dr. Trawick's research group. [44,45] For example, compound 4 was previously identified as a cathepsin L inhibitor.[46] Since cruzain shares structural similarities with cathepsin L, another cysteine protease, various TSC analogs were screened for cruzain inhibition validating the first study demonstrating cruzain inhibition by compounds bearing the TSC moiety. The proposed mechanism of action involves a nucleophilic attack by the thiolate anion, of the cysteine residue, on the electrophilic thiocarbonyl of TSC. An amine substitution of TSC are not generally tolerated in cruzain. In addition, saturation of the C=N bond, and various substitutions are not generally tolerated. However, alkyl substitution and both mono- and disubstitution yield increased potency. [25] In addition, Du et al. showed that halogen groups such as bromine and chlorine are very tolerated at the 3' and 5'-position on the aryl ring. The 3'-substituent was found in the S2 subpocket. This was confirmed in another study that also demonstrated the enhanced inhibition in presence of benzophenone. Furthermore, Fujii et al. discovered the maximal dosage associated with cytoxicity as 10 μM. Also, extension of the ethyl group resulted in subnanomolar inhibition, as low as 19 nM, therefore highlighting this for further optimization.[47] Additional functionalization of the TSC warhead involved evaluation of compound 3, one that is evaluated in my investigation, as a cruzain inhibitor, however

IC_{50} value was not reported.[48] In my experiments, this is the highest concentration of compound evaluated for dose-dependent response. Greenbaum ascertained vital structural features of cruzain based on enzyme assay results including that the 3-' and 4'-positions on the aryl ring are valuable for further optimization since the best compound with a bromine at 3' had IC_{50} value of 60 nM with a preincubation time of 5 minutes. Furthermore, substitution of 2' position was not tolerated, and any N disubstitutions on R1 (next to double bonded S) lowered compound potency. Although N disubstitutions lowered potency against cruzain, this increased antiparasitic activity suggesting aryl TSCs may act by another mechanism other than cruzain inhibition.[25] In addition to moderate inhibitory properties, the best compounds demonstrated negligible toxicity in mice after 62 hours. Therefore, aryl TSCs are potential antichagasic agents, however their mechanism of action may be more complex than cruzain inhibition. [25]

Later, novel aryl TSCs with a nitro group were evaluated as antichagasic candidates, however these showed poor correlation between cruzain inhibition and trypanocidal activity. Again, this reaffirms the suggestion that aryl TSCs are acting by some other mechanism. It is possible that the nitro group allows for oxidative stress to occur which may account for high antiparasatic activity. Interestingly, Blau et. A synthesized and screened novel aryl TSC derivatives that lacked inhibitory properties, but still retained high trypanocidal activity. The mechanism of action regarding aryl TSCs are covalent catalysis involving the thioamide group forming a covalent bond with the Cys25 amino acid where the aryl group is located in the deep hydrophobic pocket. This was confirmed through molecular docking studies showing aromatic groups in the lipophilic

S2 subpocket. Furthermore, these compounds also contain fit in S1 subsite allowing for the thiocarbonyl carbon to position near the catalytic residue Cys25.[49]

Wanderlan et. Al designed aryl and aroxyl TSCs disrupting the planarity and symmetry of original TSCs. Investigation into the cruzain inhibitory properties of T-shaped aryl and aryloxyl TSCs elucidated key structure-activity relationships. For example, fourteen of twenty-three compounds demonstrated percent inhibition of cruzain by more than 70% indicating that conformationally constrained compounds have a higher affinity for binding than less conformationally constrained ones. However, the best cruzain inhibitors wtih IC_{50} values of 0.07 ± 1.2 and 0.008 ± 1.6 μM were not active against the parasite. [50] This may be due to trouble getting past the parasitic membrane, or these compounds may act by some other mechanism.

Statement of purpose

Chagas' disease affects millions worldwide, due partly to vectorial distribution, where it is the leading cause of heart disease in Latin America. Presently, there are only two treatments available for the acute form while no treatment is established for the chronic form. Both medications are associated with deleterious side effects warranting further investigation into other possible therapeutics.

The etiological agent, *T. cruzi*, contains a cysteine protease, cruzipain, necessary throughout its life cycle, so this enzyme merits further investigation as a possible target. A murine model of acute T. cruzi infection with an irreversible inhibititor, vinyl sulfone, and cruzain, the recombinant form of cruzipain, exhibited curative characteristics validating this as a target for further therapeutic development.

The TSC compounds, cathepsin L inhibitors, have been evaluated as potent inhibitors of cruzain due to structural similarities between the two enzymes. Further optimization of the TSC warhead resulting in structural variants are investigated as potent inhibitors in this study through a fluorogenic assay. Potency is demonstrated through IC_{50} determination among advanced kinetic studies in order to explore mode of inhibition.

CHAPTER TWO

Methodology for the Biochemical Evaluation of Cruzain Inhibitors

Chemical sources and materials

Cruzain was obtained via expression in E. coli using *T. cruzi* DNA provided by Dr. James McKerrow's laboratory at University of San Francisco. The fluoregenic substrate, Z-FR-AMC and Brij 35 solution were procured from Sigma Aldrich. DMSO was purchased from Acros Chemicals. DTT was purchased from Omnipure and reconstituted in 400 mM NaOAc solution. NaOAc solution was bought from EMD Biosciences. In order to conduct the fluoregenic assay, a ThermoFluoroskan Ascent FL microplate reader and black 8x12 Corning 26 86 assay microplates (96 well) were utilized. Fluorometric data obtained from enzyme assays was analyzed using Graphpad 5.0 software. In order to weigh many compounds, a Mettler Toledo AX microbalance with an accuracy of 0.01 grams.

Preparation of reagents

Solutions such as 10% Brij solution, 40 mM sodium acetate (NaOAc) buffer (pH 5.50±0.05), ethylenediaminetetraacetic acid (EDTA), 35% dimethyl sulfoxide (DMSO), and 6 mM benzyloxycarbonyl-L-phenylalaninyl-L-argininyl-7-amino-4-methylcoumarin (Z-FR-AMC) were made using ultrapure water. The NaOAc buffer was adjusted to pH 5.5 using glacial acetic acid. TSC analogs were synthesized by members of Dr. Pinney's laboratory as part of a collaboration between his lab and Dr. Trawick's.

Serial dilutions of inhibitor solutions were made using 100% DMSO, solid compound, and ultrapure water as detailed in Table 1.

INHIBITOR	CONCENTRATION	UNITS	PREVIOUS SOLUTION (µL)	100% DMSO (µL)	TOTAL (µL)
STOCK	20	mM			
A	2	mM	20	180	200
B	200	µM	20	180	200
C	20	µM	20	180	200
D	2	µM	20	180	200
E	0.2	µM	20	180	200
F	0.02	µM	20	180	200

Table 1.Preparation of serial dilutions of compound solutions using 100% DMSO

Then varying concentrated inhibitor solutions, evaluated in enzyme assay, were prepared from these serial dilutions as described in Table 2. Inhibitor solutions from 0.00005 to 10 µM were evaluated in the fluorogenic assay for each compound.

FINAL CONC. (µM)	STOCK CONC. (µM)	SOLUTION	VOLUME (µL)	DMSO (µL)	WATER (µL)
10	200	A	10	25	65
5	100	A	5	30	65
1	20	B	10	25	65
0.25	2	C	25	10	65
0.05	1	C	5	30	65
0.005	0.02	E	25	10	65
0.001	0.02	E	10	25	65
0.00005	0.001	F	5	30	65

Table 2.Preparation of inhibitor solutions with 35% DMSO using serial dilutions from above

Preparation of cruzain solution

In each well, cruzain was suspended in solutions of NaOAc, EDTA, DMSO, Brij detergent, and DTT in order to result in final conditions as detailed in Table 3. Cruzain was added before preincubation time. The enzyme was initially thawed in ice before aliquoted into solution.

COMPOUND	FINAL CONCENTRATION	UNITS
NAOAC	100	mM
EDTA	1	mM
DTT	2.5	mM
SUBSTRATE	15	mM
ENZYME	0.1	nM
DMSO	2%	
BRIJ	0.01%	

Table 3.Concentration of substances in each well

Enzyme assay

A series of TSC derivatives were evaluated as potent inhibitors by obtaining IC_{50} values. Further kinetic studies elaborated on nature of inhibitors such as if these compounds are time-dependent or slowly binding. All studies involved a fluorogenic enzyme assay involving cruzain and fluorogenic peptide substrate, Z-FR-AMC. Enzmatic activity was evaluated through the cleavage of scissile bond as illustrated in Figure 8.

Cruzain's activity is demonstrated through the hydrolysis of the peptide bond in Z-FR-AMC releasing the fluorogenic product, AMC. The production of AMC is monitored over time resulting in an enzymatic rate obtained from measurement of fluorescence using a microplate reader.

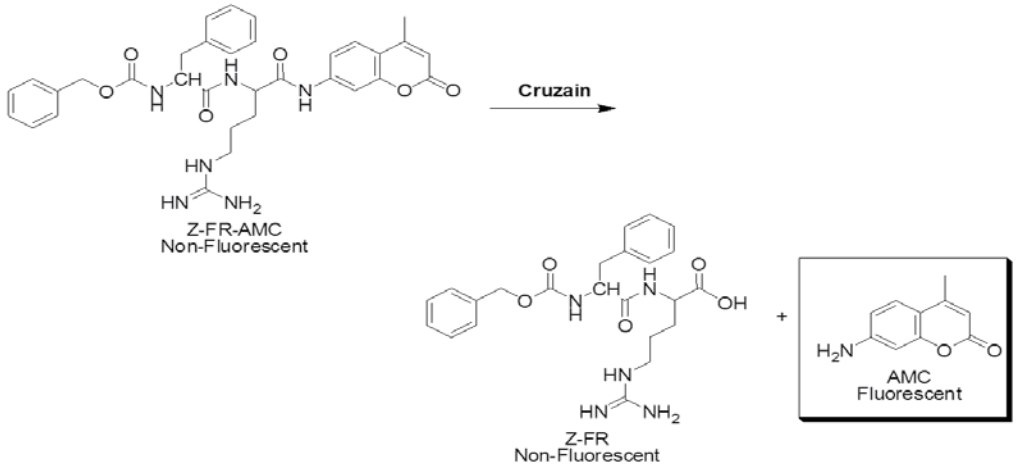

Figure 8.Fluorogenic reaction of cruzain with peptide substrate Z-FR-AMC

The assay involves enzyme solution, assay buffer, 15 μM Z-FR-AMC solution, and 35% DMSO. Assay buffer is prepared as described in Table 4 in order to exact appropriate final concentrations of each substance shown in Table 3. Enzyme solution,

previously described above, is further described in Table 5 in accord with resulting final conditions as listed in Table 3.

COLUMNS	VOLUME (µL)	EDTA (µL)	DTT (µL)	NAOAC (µL)	WATER (µL)	BRIJ (µL)
1	1000	32.500	40.625	325.000	600.575	1.3
2	2000	65.000	81.250	650.000	1201.150	2.6
3	3000	97.500	121.875	975.000	1801.725	3.9
4	4000	130.00	162.500	1300.00	2402.300	5.2
5	5000	162.50	203.125	1625.00	3002.875	6.5

Table 4.Volumes of each substance in columns for assay buffer

COLUMN	VOLUME (µL)	EDTA (µL)	DTT (µL)	NAOAC (µL)	WATER (µL)	BRIJ (µL)	CRUZAIN (µL)
1	1000	32.500	40.625	325.000	600.575	0.6	0.155
2	2000	65.000	81.250	650.000	1201.150	1.2	0.313
3	3000	97.500	121.875	975.000	1801.725	1.8	0.471
4	4000	130.00	162.500	1300.00	2402.300	2.4	0.629
5	5000	162.50	203.125	1625.00	3002.875	3.0	0.787

Table 5.Volumes of each substance in columns for enzyme solution

Determination of AMC calibration curve

An AMC calibration curve was determined to calibrate the instrument. In order to construct an AMC curve, relative fluorescence units (RFU), measuring fluorescence, is plotted on y-axis for a range of substrate concentrations, including the concentration utilized in the enzyme assays, against time.

In this experiment, 6 mM AMC solution was made by dissolving 3.96 mg AMC in NaOAc buffer. Serial dilutions of 6 mM AMC solution were prepared to evaluate a range of [AMC] from 15 to 0.5 µM as detailed in Table 6.

AMC SOLUTIONS	CONC. (µM)	WATER (µL)	DMSO (µL)	AMC (µL)	AMC SOLUTION
STOCK	6 mM	0	1000	3.896 mg	
A	150	975.0	0.00	25.00	Stock
B	100	325.0	8.30	666.70	A
C	75	243.75	6.25	750.0	B
D	50	325.00	8.30	666.7	C
E	25	487.50	12.50	500.0	D
F	10	585.00	15.00	400.0	E
G	7.5	243.75	6.25	750.0	F
H	5	325.00	8.30	666.7	G
I	2.5	487.50	12.5	500.0	H

Table 6.Preparation of AMC dilutions

Assay buffer was prepared with NaOAc buffer solution, DTT, EDTA, Brij, and ultrapure water. In addition, a 35% DMSO solution was prepared with DMSO and ultrapure water. Then, a micro plate reader measured the fluoroscence of Z-FR-

AMC. (ThermoFluoroskan Ascent FL). An 8*12 tray (13 96 Wells Costar) is used to hold the enzyme assay solution.

After placing these solutions into wells, conditions were set for measurements. Preincubation of inhibitor with enzyme lasted for 5 minutes. Temperature was set at 25°C and at different times, the solutions were agitated for 10 seconds at 1200 RPM. One measurement was taken where the measurement was repeated every 15 seconds for 21 measurements of each well with emission: excitation wavelength of 355 nm: 460 nm. These conditions are replicated for all enzyme assays. This was adapted from a previous protocol because it showed the best conditions for optimal enzymatic activity.

Determination of K_M

A Michaelis-Menten curve was constructed in order to indicate substrate affinity for cruzain and calibrate the instrument. The Michaelis-Menten curve allows us to identify enzymatic activity by plotting fluorescence measured in RFU against time of varying substrate concentrations. It is important to note that enzyme solution is present.

Preparation for enzyme assay is similar to one used for AMC calibration curve with addition of enzyme solution preparation. Also, serial Z-FR-AMC dilutions are prepared, instead of serial AMC solutions, as depicted in Table 7.

SUBSTRATE SOLUTIONS	CONC. (µM)	WATER (µL)	DMSO (µL)	SUBSTRATE (µL)	SUBSTRATE SOLUTION
STOCK	6 mM	0	1000	3.896 mg	
A	150	975.0	0.00	25.00	Stock
B	100	325.0	8.30	666.70	A
C	75	243.75	6.25	750.0	B
D	50	325.00	8.30	666.7	C
E	25	487.50	12.50	500.0	D
F	10	585.00	15.00	400.0	E
G	7.5	243.75	6.25	750.0	F
H	5	325.00	8.30	666.7	G
I	2.5	487.50	12.5	500.0	H

Table 7.Preparation of serial Z-FR-AMC dilutions

Assay buffer, cruzain solution, and 35% DMSO solution were prepared as previously described above. All solutions were placed in ice until required for analysis in order to ensure enzymatic integrity. Assay buffer, 35% DMSO, and cruzain solution were added to wells in that order. Final concentrations of each component are shown in Table 3. After a 5-minute preincubation period, Z-FR-AMC solutions ranging from 15 µM to 0.5 µM were added to each well. Incubation period allowed for enzyme and inhibitor to adjust before beginning reaction with substrate. After addition of substrate, measurement of fluorescence over time was taken. Enzyme assays were run in triplicates.

Determination of IC_{50}

In order to evaluate the inhibitory properties of each compound, a value referred to as IC_{50} was obtained. This is the concentration of inhibitor that inhibited the maximal

velocity by 50%. To obtain this value, a range of concentrations of each compound was tested compared to the control. Inhibitor solutions from 10 μM to 0.00005 μM for respective compounds were prepared as previously described above in Table 2. Enzyme and assay buffer solution were also made as previously described above. A 15 μM Z-FR-AMC solution was also prepared.

Assay buffer and inhibitor solutions were added to each well in that order. For control, 35% DMSO was added in lieu of inhibitor solutions. After thawing enzyme, cruzain was mixed gently before adding appropriate amount into enzyme solution. This was further mixed gently before adding into each well. This was allowed to incubate for 5 minutes in order for the compound and enzyme to bind. Then, substrate was added to initiate the reaction. The fluorometric instrument (Thermoskan Ascent FL) recorded enzymatic cleavage of Z-FR-AMC.

Determination of time-dependence

A progress curve was obtained for each compound. Secondly, an IC_{50} curve with varying preincubation times from 5 minutes to 120 minutes was identified for various compounds in order to assess time-dependence. Each was obtained through fluorogenic enzymatic assay using ThermoFluoroskan Ascent FL microplate reader and analyzed using Graphpad 5.0 software. Atleast two sets of triplicates were used for data analysis.

Determination of progress curve

In order to determine the time-dependence of inhibitors, a progress curve was generated. Enzyme solution, assay buffer, 35% DMSO solution, and titrated inhibitor solutions were prepared from 0.00005 μM to 10 μM. A microplate fluorimeter and 13 96

8 x 12 (Costar) plate is used for the fluorogenic enzyme assay. After assay buffer, inhibitor solutions, 35% DMSO solution, and enzyme solution is added in that order, then 15 μM Z-FR-AMC solution is added to initiate the reaction. Measurements are recorded using a fluorometric microplate reader. Measurements are taken for an hour. Through linear regression analysis utilizing Graphpad 5.0 software, a progress curve is obtained.

Varying pre-incubation times

Varying preincubation times also establishes time-dependence. Preincubation time refers to time allotted for inhibitor binding to cruzain before substrate is added. Enzyme assay solutions, assay buffers solutions, inhibitor solutions, 35% DMSO solution, and substrate solutions were prepared as previously described. A fluorogenic assay was conducted as previously described with a pre-incubation time of 5 minutes. This was repeated for different pre-incubation times: 0, 5, 30, 60, and 120 minutes.

CHAPTER THREE

Results

Biochemical evaluation of potential cruzain inhibitors

This chapter will present the results of the biochemical evaluation of a series of seven TSC derivatives (compounds 1,2 and 4-8) synthesized by Dr. Erica N. Parker and (compound 3) Dr. Lindsay Jones of Dr. Kevin G. Pinney's laboratory as part of a collaboration between Dr. Trawick's and Dr. Pinney's groups at Baylor University.[46,51–54]

TSC derivatives were initially synthesized as inhibitors of cathepsin L. Cathepsin L is structurally similar to cruzain, therefore cathepsin L inhibitors may also serve as cruzain inhibitors. This was proven in work of Du et al.[17] For this thesis, a series of TSC derivatives were synthesized and screened as potential cruzain inhibitors. Initially, these compounds were evaluated at 10 μM for percent inhibition. Compounds with percent inhibition greater than 50% went onto further testing. Further testing consisted of obtaining IC_{50} values by constructing a dose-response curve at varying preincubation periods. Also, progress curves and K_i values were obtained.

Enzyme assay

The enzymatic assay employed for kinetic determination monitors the cleavage of the scissile bond in the fluorogenic peptide substrate, Z-FR-AMC, releasing the fluorogenic product, AMC over time as shown in Figure 8. This bond cleavage is demonstrative of cruzain activity. The rate of product formation over time is calculated

through linear regression analyses using GraphPad Prism software version 5.0. As illustrated in Figure 9, enzymatic activity, measured in RFU, is monitored over time for varying concentrations of inhibitor.

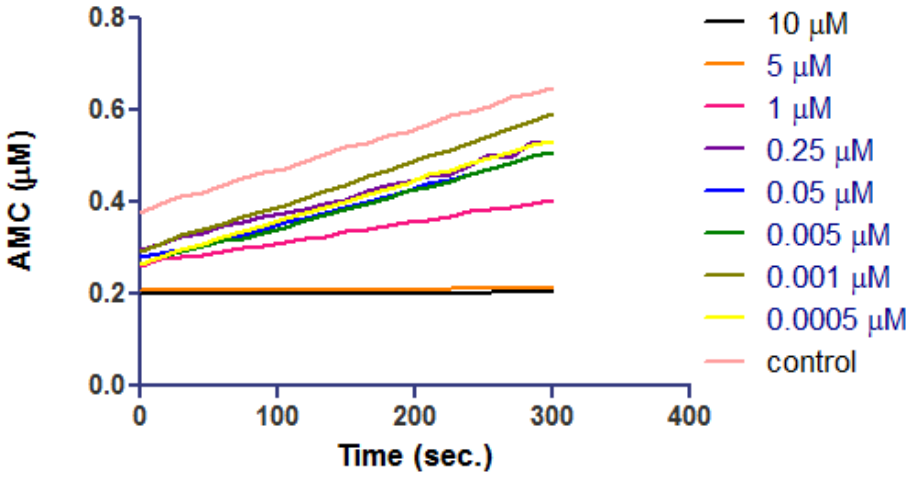

Figure 9.Representative depiction of cruzain activity with varying concentrations of an inhibitor

AMC curve

An AMC curve is constructed in order to calibrate the instrument. Different concentrations of AMC solutions are mixed with assay buffer. Fluorescence is monitored for 5 minutes at conditions used for enzyme assay. These conditions are 25° C, agitated every 10 seconds at 1200 RPM between each measurement, and observed at excitation and emission wavelengths of 355 and 460 nm, respectively. Assays were run in triplicates. Linear regression analysis imposes a line of best fit onto data.

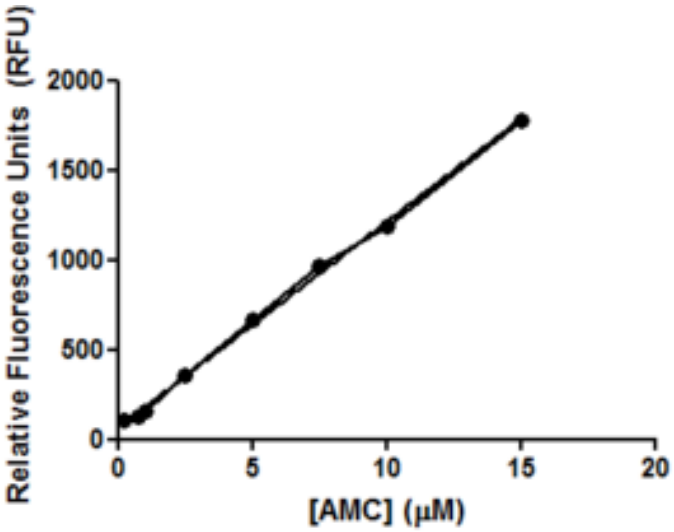

Figure 10. AMC calibration curve
(relative fluorescence units v. [AMC])

Determination of V_{max} and K_m of Z-FR-AMC and cruzain

A Michaelis-Menten plot is constructed in order to assess the concentrationos substrate that reduces maximal reaction velocity by half. Kinetic values such as K_m and V_{max} are obtained as displayed on the Michaelis-Menten plot constructed in Figure 11.

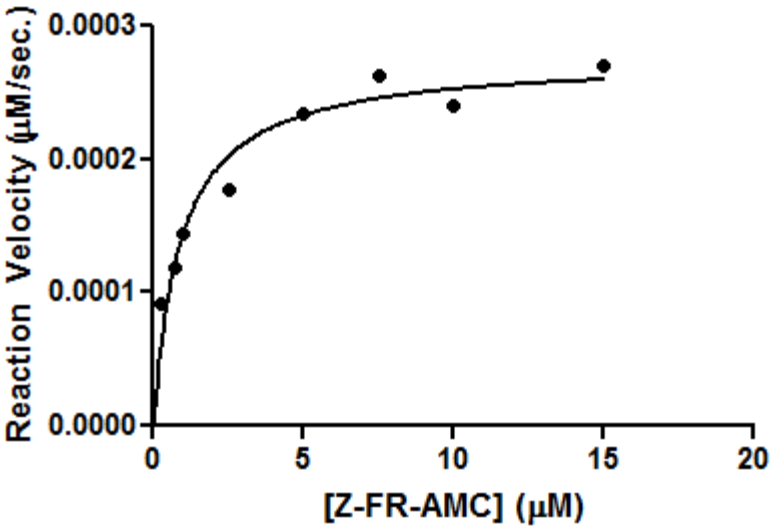

Figure 11. Michaelis-Menten plot

Reaction velocity is plotted on y-axis while concentrations of substrate are plotted on x-axis. Through non-linear regression analysis with GraphPad Prism software 5.0, data was analysed the Michaelis-Menten equation in order to exact V_{max} and K_m values. Therefore, these values were obtained by measuring cruzain activity at fixed enzyme concentration while varying concentration of substrate.

$$v_0 = \frac{dP}{dt} = \frac{V_{max}[S]}{K_m + [S]} \qquad \text{Equation 1}$$

Since cruzain reaction velocity increases as substrate concentration increases until it obtains V_{max}, it follows Michaelis-Menten equation. Consequently, K_m refers to the substrate concentration associated with half-maximal reaction velocity and V_{max} refers to the maximal reaction velocity associated with excess substrate concentrations. The K_m value was 2.35±0.27 µM. The V_{max} was 0.099 µM/sec.

Determination of inhibitory activity

In order to ascertain potent inhibitors, percent inhibition was first obtained of all compounds. Percent inhibition was determined by conducting fluoregenic assay of each compound at 10 μM. Enzymatic reaction velocity was monitored with each compound for 5 minutes using Thermo Fluoroskan Ascent Fluorescence plate reader. Then, experimental data was fitted into percent inhibition equation as illustrated below using GraphPad Prism software 5.0. K refers to fluorescence of control, without inhibitor while Y refers to fluorescence of each solution of compound.

$$Y = \left(\frac{K-Y}{K}\right) \times 100\% \qquad \text{Equation 2}$$

As shown in Table 8, four of the eight compounds had percent inhibition less than 50% while the other four compounds had percent inhibition greater than or equal to 50%. The compounds that fall in the latter group went onto further testing.

Compound Number	Structure	Percent Inhibition ± SE
1	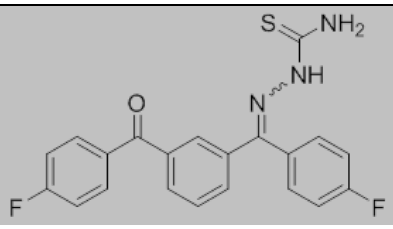	99.1±0.9
2	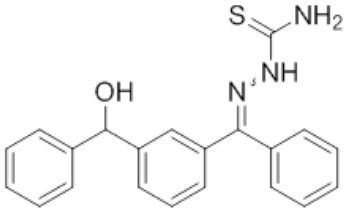	97.0±1.4
3	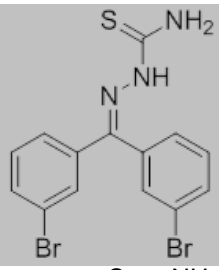	98.6±0.1
4	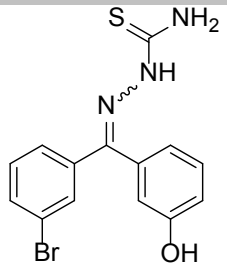	99.7±0.2
5	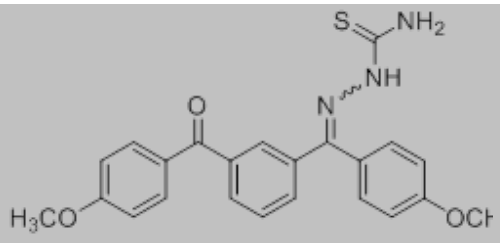	61.8 ± 4.8

Compound Number	Structure	Percent Inhibition ± SE
6	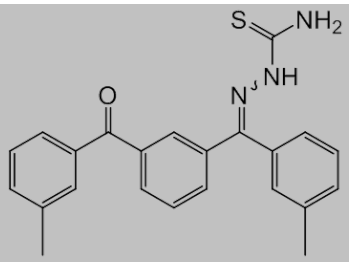	100
7	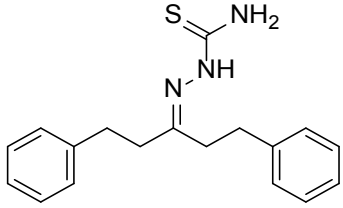	23.3±2.4
8	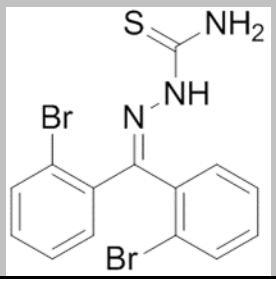	22.3±0.8

Table 8. Determination of percent inhibition of TSC derivatives

Compounds with percent inhibition greater than or equal to 50% were evaluated for potency. Here, potency was demonstrated through IC_{50} values which refers to the inhibitory concentration required to reduce maximal reaction velocity by 50%. This was determined with a fluoregenic assay. Titrations of each compound were prepared in DMSO and eight inhibitor dilutions ranging from 0.00005 µM to10 µM were incubated with cruzain in the assay buffer for 5 minutes before reaction was initiated with addition of 20 µL of 15 µM substrate Z-FR-AMC. Activity was monitored using the Thermo Fluoroskan Ascent Fluorescence plate reader. Again, the fluorescence was detected at an

excitation and emission wavelength of 355 nm and 460 nm, respectively, at 25°C for 5 minutes.

Experimental data, as shown in Figure 9, were fitted into the Hill slope equation as described below. This nonlinear regression analysis was conducted using GraphPad Prism software version 5.0. In particular, the logarithm of concentration of inhibitors was plotted with reaction velocities in order to construct a sigmoidal curve using a variable slope model. The Hill slope refers to the slope of curve.

$$Y = Bottom + \frac{(Top - Bottom)}{1 + 10^{(log\,IC_{50} - x) * HillSlope}} \qquad \text{Equation 3}$$

In equation listed above, Y refers to initial velocity at different concentrations of inhibitor whereas V_{min} and V_{max} refer to lowest reaction velocity associated with highest inhibitor concentration and highest reaction velocity associated with lowest inhibitor concentration, respectively. As shown in Figure 12 , this IC_{50} curve refers to compound 4. Although visual inspection of data analysis results in $LogIC_{50}$, it is preferable to determine this through nonlinear regression analysis.

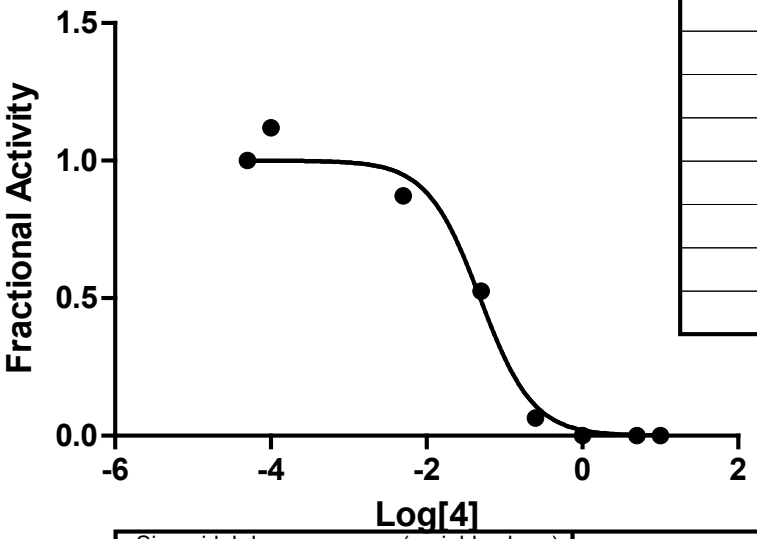

Conc. (μM)	slopes
1.000	0.000
0.699	0.000
0.000	0.000
-0.602	0.065
-1.301	0.526
-2.301	0.872
-4.000	1.120
-4.301	1.000

Sigmoidal dose-response (variable slope)	
Best-fit values	
Bottom	= 0.0
Top	= 1.000
LogEC50	-1.312
HillSlope	-1.280
EC50	0.04872
Std. Error	
LogEC50	0.08057
HillSlope	0.3179
95% Confidence Intervals	
LogEC50	-1.509 to -1.115
HillSlope	-2.058 to -0.5024
EC50	0.03094 to 0.07672
Goodness of Fit	
Degrees of Freedom	6
R square	0.9858
Absolute Sum of Squares	0.02394
Sy.x	0.06316
Constraints	
Bottom	Bottom = 0.0
Top	Top = 1.000
Number of points	
Analyzed	8

Figure 12. General IC_{50} determination with the dose-response sigmoidal model for compound 4 from GraphPad Prism 5.0 Software

The average IC_{50} values of evaluated compounds are shown in Table 9

Table 9 and a representative data analysis for each compound is described in APPENDIX *B*. Note these are associated with preincubation time of 5 minutes.

Compound Number	Structure	IC_{50} ±SE (nM)
1	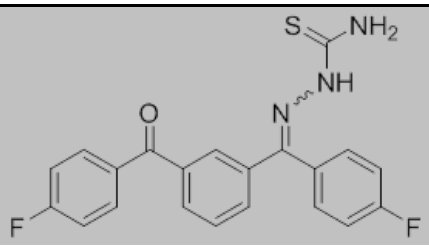	45.9±4.1
2	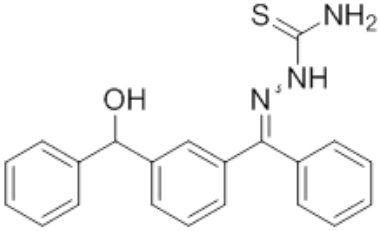	1248 ±156.9
3	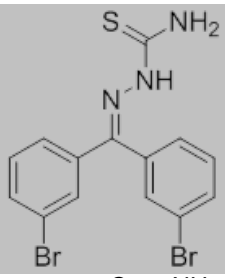	20.2
4	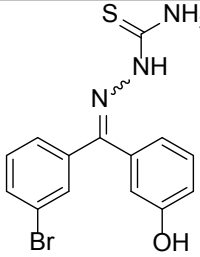	32.0±4.0

Compound Number	Structure	IC_{50} ±SE (nM)
6	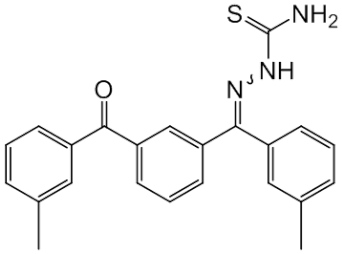	217.1±45.2

Table 9. IC_{50} values

Progress curves

Three of the eight compounds were evaluated for time dependence. A range of inhibitor concentrations were prepared in DMSO and mixed with assay buffer, enzyme, and substrate Z-FR-AMC in that order. Final assay conditions were 1 mM EDTA, 0.01% Brij, 2.5 mM DTT, 100 mM NaOAc, 2% DMSO, 0.1 nM cruzain, and 15 μM Z-FR-AMC. There was no incubation time. The reaction was monitored over 1 hour with excitation and emission wavelengths of 355 nm to 460 nm, respectively, at 25°C. Enzyme assays were run twice in triplicates in most cases.

Linear regression of experimental data yielded in construction of progress curve. The progress curve of compound 1 is illustrated in Figure 13. Time identified in seconds is plotted on x-axis while concentrations of AMC are plotted on y-axis. Each line corresponds with a different concentration of inhibitor. Progress curves were obtained for compounds 1-3.

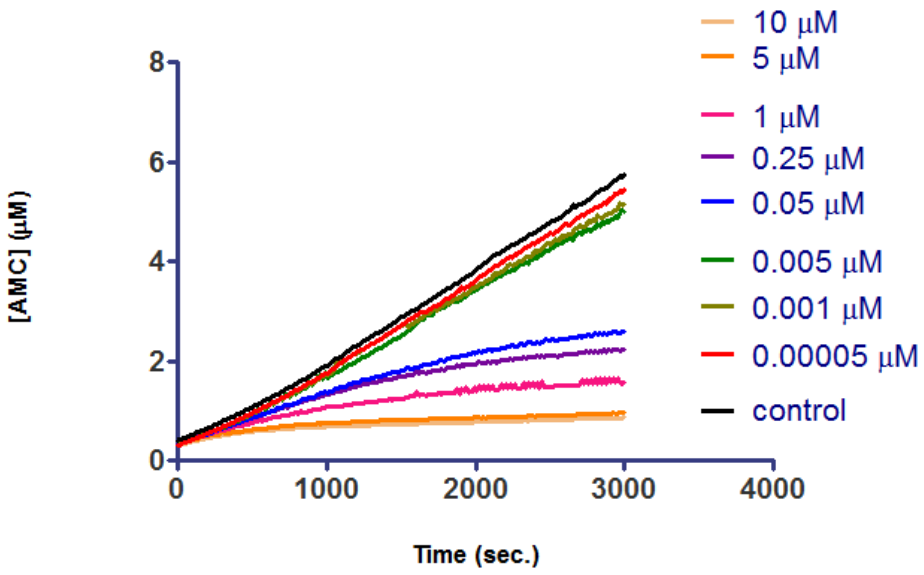

Figure 13. Progress curve of compound 1

Varying pre-incubation times

After assessing time-dependence, the effect of increasing preincubation times on IC_{50} values was evaluated by constructing sigmoidal-dose curve responses for preincubation times of varying periods. Respective sigmoidal dose curve responses were plotted on one graph in order to exact a visual depiction of the effect. Only compounds 1,2 and 4 were evaluated for this outcome.

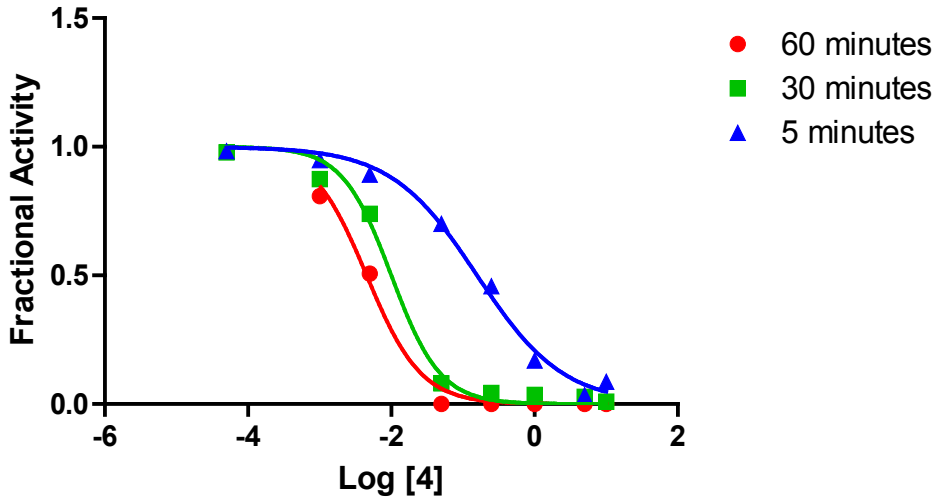

Figure 14. Determination of IC_{50} values for varying preincubation times with compound 4

The effect of varying preincubation times for compound 4 is illustrated in Figure 14. There is a decrease in IC_{50} values as preincubation time increases. This result is also seen for respective compounds as illustrated in APPENDIX E.

Determination of K_i

The data used to construct the sigmoidal curve for IC_{50} values are also used to obtain K_i data, inhibition constant values, by fitting the data into the Morrison equation. This is used to indicate if the compound is tight-binding. It also applies to transient covalent bond formation. Respective K_i values are shown in Table 10. These values were obtained for four compounds. Compound 4 was associated with the lowest K_i value of 4.7±0.1 nM.

Compound	Structure	K_i ± SE (nM)
1	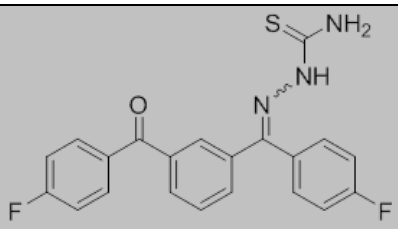	8.0±0.1
2	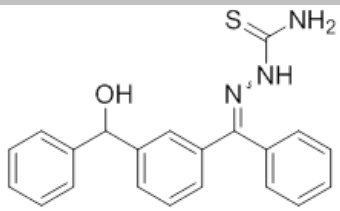	100.0±3.7
3	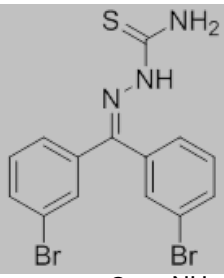	46.9±11.3
4	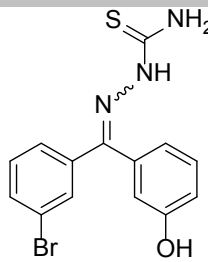	4.7±0.1
6	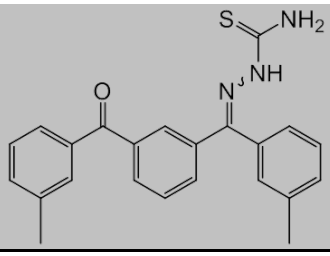	47.6±1.4

Table 10.K_i values

As illustrated in equation below, the inhibition constant, K_i, depends upon multiple variables such as total concentration of enzyme, $[E]_T$, total concentration of inhibitor, $[I]_T$, concentration of substrate, [S], Michaelis-Menten constant, K_M , initial

velocity,v_0 , and inhibited velocity, v_i . For the Morrison equation, substrate concentration is 15 μM, K_M is equal to 2 μM, initial velocity is 1 μM/seconds, and total enzyme concentration is 0.1 nM. The total concentration of inhibitor refers to serial dilutions of inhibitor ranging from 0.00005 to 10 μM. Inhibited velocity refers to the enzymatic reaction rate of the cleavage of Z-FR-AMC for each concentration of inhibitor. This is determined experimentally as the production of the fluorogenic component, AMC, is produced by peptide cleavage over time. The production is measured in units of fluorescence by Thermo Fluoroskan Ascent Fluorescence plate reader. Then, linear regression analysis, available through GraphPad Prism software version 5.0, determines the slope as a function of time.

$$\frac{v_i}{v_o} = 1 - \frac{([\mathrm{E}]_T + [I]_T + (K_I(1 + \left(\frac{[S]}{K_M}\right)) - \sqrt{([\mathrm{E}]_T + [I]_T + (K_I\left(1 + \left(\frac{[S]}{K_M}\right)\right))^2 - 4[E]_T[\mathrm{I}]_T}}{2\,[E]_T}$$

Equation 4

Then, this is used to construct a curve as shown below. Concentration of compound is plotted on x-axis and fractional activity is plotted on y-axis. Additional constraints were placed upon the data, Morrison, and IC_{50} equation like the top y value cannot exceed 1.0 and the bottom y value cannot be less than 0.0.

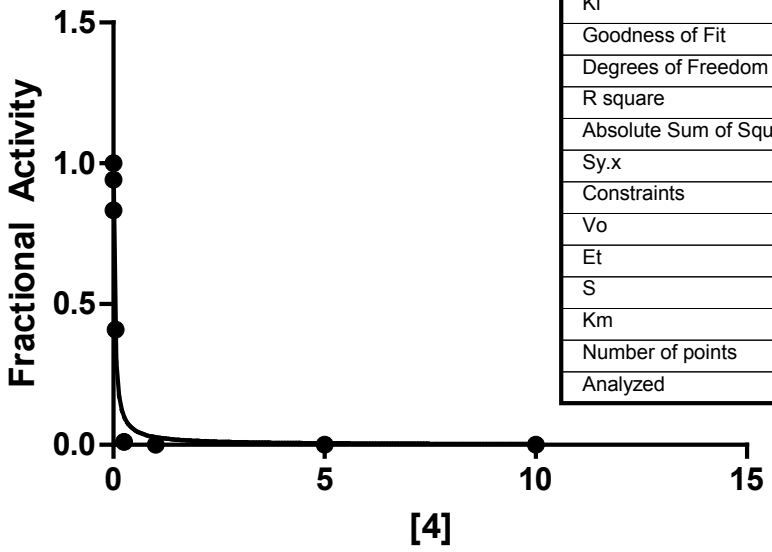

Morrison Ki	
Best-fit values	
Vo	= 1.000
Et	= 1.000e-005
Ki	0.004684
S	= 15.00
Km	= 3.000
Std. Error	
Ki	0.0007651
95% Confidence Intervals	
Ki	0.002875 to 0.006494
Goodness of Fit	
Degrees of Freedom	7
R square	0.9900
Absolute Sum of Squares	0.01466
Sy.x	0.04576
Constraints	
Vo	Vo = 1.000
Et	Et = 1.000e-005
S	S = 15.00
Km	Km = 3.000
Number of points	
Analyzed	8

Figure 15. Graphical representation of Morrison equation

The curve fit to the Morrison equation for compound 4 is shown in Figure 15. Discussion of results of biochemical evaluation of TSC analogs are presented in Chapter 4.

CHAPTER FOUR

Discussion

This chapter will present a discussion of the results of the biochemical evaluation of bromobenzophenone and benzoylbenzophenone TSC derivatives.

The results of this study are summarized in Chapter 3, specifically in Table 8-10. The bromobenzophenone compound 4, from the library tested, was previously reported as a non-peptidic inhibitor of cathepsin L with IC_{50} values of 188.7 nM.[46] However, this compound was evaluated against cruzain for the first time in this study. In addition, the other six compounds were evaluated for cruzain inhibitory properties for the first time here. Out of the eight compounds, compounds 1-4 and 6 demonstrated nanomolar inhibition of cruzain. The mode of inhibition was further explored for compounds 1-4. Compound 4 demonstrated inhibitory properties, time-dependence, and tight-binding inhibition or transient covalent bond formation.

The peptidic substrate, Z-FR-AMC, was chosen as a result of its high affinity for cruzain. Since the cleavage of the substrate yields in Z-FR, a non-fluorogenic component, and AMC, a fluorogenic product, then the reaction rate can be monitored through the fluorescence of the fluorogenic product over time. This substrate is a specific substrate for cruzain because the enzyme preferentially cleaves after phenylalanine and arginine residues. A calibration curve was used in order to assess the integrity of fluorimeter (Thermo Fluoro Askan FL microplate reader). The calibration curve is shown in Figure 10. As illustrated, the equation was used in order to relate measurements of fluorescence and concentration of AMC. The y-intercept represents the measurement of fluorescence

at zero concentration of substrate. The calibration curve allows for the conversion of AMC to RFU.

Afterwards, a Michaelis Menten curve was constructed, as shown in Figure 11, in order to further assess the integrity of the assay. The Michaelis-Menten constant, K_m, describes the concentration of substrate associated at half maximal reaction velocity. A common enzyme kinetic model is illustrated below.

$$E + S \rightleftarrows ES \Rightarrow E + P$$

Certain assumptions are established such as i) steady-state approximation, ii) free ligand approximation, and iii) rapid equilibrium approximation where $k_{cat} << k_{off}$. The constant, k_{cat},is the rate constant for the conversion of enzyme-substrate complex, ES, to product P and enzyme E, and k_{off} is the rate constant for the breakdown of ES complex to E and substrate, S. A low K_m indicates this substrate has a high affinity for cruzain.[55] Here, the K_m value is 2.3 ± 0.3 μM.

The materials utilized in enzyme assays were selected based on a previous protocol. Enzymatic structure can be disrupted due to a drastic change in temperature, pH, and addition of denaturing agents. Once the structure is disrupted, then enzymatic activity is affected. A reducing agent, DTT, also commonly referred to as Cleland's agent, was chosen in order to prevent oxidation to disulfide bonds. DTT will become oxidized as opposed to cruzain's thiol group. These general chemical properties validate the appropriate use of this reagent in this essay. A chelating agent, EDTA, is used in this essay because it chelates metal ions that might interfere with enzymatic activity and precipitate solutions. An amphiphilic surfactant, Brij, is used in order to prevent enzyme aggregation. DMSO, an organic solvent, dissolves the substrate and compound in

solution. An assay buffer is used in order to resist changes in pH of solutions. The pH of this buffer is 5.5 ± 0.5. A drastic change in pH may result in reduced enzymatic activity. This will skew results leading to errant conclusions about the potency of an inhibitor. The enzyme was obtained through recombinant DNA by Dr. Wara Arispe and the plasmid was generously provided by Dr. James McKerrow's laboratory, in *E. coli* cells. These materials ensure optimal activity for enzyme.

In order to assess potency, all compounds were subjected to enzyme assay at 10 μM in order to assess their percent inhibition. In this experiment, percent inhibition was defined as inhibition of cruzain activity by 10 μM of compound. Compounds that exhibited greater than 50% inhibition were nominated for further determination of potency. Compounds 7 and 8 did not inhibit enzymatic reaction by ≥50%, so these did not undergo further studies. An alkyl derivative, compound 7 bears the TSC warhead along with two aryl rings. It is suggested that alkyl chains off of the parent thiosemicarbazide group reduces potency against cruzain.[47] Since compound 7 exhibited poor inhibition, this suggestion is supported here. Compound 8 is a dibromo substituted benzophenone where bromine substitution occurs at *ortho* position on one ring and another substitution occurs at an *ortho* position on another ring. Previous studies showed that disubstitutions exhibit poor potency against cathepsin-L.[56] Since cruzain is structurally similar, this may indicate the reason for poor inhibition.

Potency is further demonstrated through IC_{50} values. IC_{50} refers to the inhibitory concentration that inhibits the maximal reaction velocity by 50%. In concentration-response plots for determination of IC_{50}, it is assumed that the inhibitor is binding to only one site. Fractional activity, a direct ratio of concentration of free enzyme to total

concentration of enzyme, is plotted against the logarithmic concentration of inhibitor. Compounds 1-4, and 6 were evaluated for IC_{50} value with five minute preincubation time. An increase in inhibitor concentration should result in a decrease of enzymatic activity. This is in accord with enzyme kinetic model. The most potent compound was compound 3 with an IC_{50} value of 20.2 nM. This benzophenone compound contained dibromo substitutions at the *meta* positions of each aromatic ring. The least potent compound of the evaluated series was compound 2 with an IC_{50} value of 1248 nM.

It appears that the presence of a hydroxyl group instead of a carbonyl group reduces the potency, however additional studies are warranted. Possible examination of potency of an unsubstituted benzoyl benzophenone analog can help distinguish the effect of that carbonyl on potency. Interestingly, compound 5 bears striking resemblance with compounds 1 and 6 except substitution varies. Compound 1 contains a fluoro group while compound 5 contains a methoxy group. Recall that the methoxy group is an *ortho*- and *para*-directing activator. Here, the methoxy groups are located in the *para* position on two different benzyl rings. Compound 6 contains two methyl groups at the *meta* position on two different aryl rings. Compound 5 did not demonstrate potent inhibition at 10 μM. Therefore, an IC_{50} value was not obtained for this compound. However, compound 1 demonstrated excellent nanomolar affinity. Based on structural differences between compounds 1 and 5, it seems the *meta*-substitution of electron-withdrawing groups significantly reduces the potency. Evaluation of a third compound with a similar electron-withdrawing group would confirm or refute this. Also, compound 6 exhibited poor inhibition at 10 μM, thereby suggesting that *meta* substitutions reduces potency. Again, further studies of compounds with variations at the *meta* position would confirm or refute

this. The dibromosubstituted compound exhibited greater potency than the monobromosubstituted one suggesting bromine substitution increases potency. It is important to note the primary structural difference between compounds 3 and 4 lies in the *meta* position of a phenyl ring. Compound 3 has a bromine at this position where compound 4 has a hydroxyl here. This suggests that placing electron-withdrawing group reduces potency, however the difference in IC_{50} values is not numerically significant to corroborate this.

It is important to note that primary structural differences between compounds 1 and 2 are the presence of the fluoro groups in compound 1 and the presence of a hydroxyl group in compound 2 instead of a carbonyl oxygen. Compound 2 is also very similar to compound 5. The main structural differences between these two compounds are the presence of a methoxy group in compound 5 and the presence of a hydroxyl group in compound 2 instead of a carbonyl oxygen.

After demonstrating potency, selected compounds were evaluated for time-dependence. Time dependence can be illustrated in a progress curve. Titrated compounds were co-incubated with enzyme and substrate without any preincubation time. The reaction was monitored for 1 hour. Initially, the enzyme is releasing the fluorogenic product, AMC, so the initial rate can be discerned from measurements of fluorescence which is later converted to concentration of AMC. For the progress curve, the reaction was monitored for one hour. As shown, as time approaches the hour, the curve levels off suggesting either substrate depletion or steady-state equilibrium. The curve levels off as the reaction rate decreases. This is related by the decrease in fluorescence measurements by the fluorimeter. Also if one concentration of inhibitor is examined, there is an increase

in enzymatic activity as represented by the slope as time increases. This confirms the dose-responsive inhibitory properties of inhibitor. Compounds 1-3 were evaluated for time-dependence.

Compound 1 is a time dependent inhibitor as suggested by progress curve shown in Figure 13. The progress curve of compound 1 with varying concentrations of compound 1 shows a decrease in the change in product formation over time as time increases. In other words, there a decrease in the change of slope indicating inhibitor binds in a time-dependent manner. Interestingly, at lower concentrations, there is an insignificant decrease in change of slopes over time suggesting that this compound is not time-dependent. However, at greater concentrations of inhibitor, there is a visible decrease in change of slopes confirming its time-dependence. Compound 2 was also identified as a time-dependent inhibitor based on the progress curve for this derivative. As time increases, there is an increase in inhibition after approximately 1000 seconds as visualized in the progress curve found in APPENDIX C. Again, this increase in inhibition is specifically seen in the decreasing slope as time approaches one hour. Compound 3 is also a time-dependent inhibitor since there is a decrease in change of slopes over time for each concentration of inhibitor. The progress curve for this compound illustrates this time dependence almost immediately. Compounds 1,2, and 4 were subjected to further studies in order to investigate this time-dependent nature. After establishing the time-dependent nature of compound 1, the manner of time-dependence was evaluated through constructing IC_{50} curves with varying preincubation times of 5, 30, and 60 minutes for compound 1 in which the IC_{50} values are 45.9, 10.6, 3.9, and 5.3 nM, respectively. There is an overall decrease in IC_{50} values as preincubation time increases. This is also visually

depicted in graph of sigmoidal dose-response curves for varying preincubation times, found in APPENDIX E, where a leftward shift of IC_{50} curves indicate the decrease in IC_{50} values as preincubation time increases. Oddly, there was not a decrease in IC_{50} value from 60 to 120 minutes. This may suggest steady-state equilibrium, or the compound is a reversible inhibitor where after 60 minutes, the compound dissociates from the enzyme. Further studies are warranted to investigate this further. If no decrease in IC_{50} values accompanied the increase in preincubation time, then this would not be considered as a slow-binding inhibitor. However, since there is a general decrease in IC_{50} values with an increase in preincubation times, then this is indicative of slow-binding. The decrease in IC_{50} values indicates that the concentration of inhibitor required to reduce maximal reaction velocity by 50% decreases as more time is given for the inhibitor to bind to enzyme. This is desirable for clinical applications since less may be given to induce an effect upon cruzain, a validated target for Chagas' disease. Compound 2 shows a decrease in IC_{50} values as seen in the graph depicting sigmoidal dose-response curves for varying preincubation times of 0,5,30,60, and 120 minutes found in APPENDIX E.

Compound 4 is also time-dependent as illustrated in Figure 14. Sigmoidal dose-response curves for preincubation times of 5, 30, and 60 minutes are shown. As preincubation time increases, there is a leftward shift of IC_{50} curves accompanied by a decrease in IC_{50} values illustrating its time-dependence. Interestingly, there is a slight decrease in IC_{50} values as preincubation time increases from 30 to 60 minutes. This may indicate that an increase in preincubation from 60 to 120 minutes would result in a negligible decrease in IC_{50} values. This may point to a possible time for which compound

takes to inhibit reaction until it reaches steady-state equilibrium. Compounds 1-4, and 6 advanced for further kinetic determination due to their potency.

In order to elucidate the mode of inhibition, K_i values, inhibition constants, were determined for potent compounds 1-4, and 6 via the Morrison equation. In order to affirm tight-binding inhibition, data obtained for a sigmoidal dose-response curve, is worked into the Morrison equation. It is normally assumed that the concentration required to reduce the enzymatic reaction by 50% is in excess of the final concentration of enzyme in reaction mixture. It is also assumed that the total concentration of inhibitor is equal to the concentration of free inhibitor, compound that is not bound to enzyme as illustrated below. The apparent K_i constant or apparent dissociation constant, is assumed to equal the total concentration of enzyme if the inhibitor has high affinity for the enzyme.

$$[I]_T = [I]_f + [EI]$$

Often, slow-binding inhibitors are tight-binding as well. Therefore, it is reasonable to suggest that these time-dependent inhibitors will be tight-binding. After compound 1 was established as a time-dependent, slow-binding inhibitor of cruzain, it was determined to be a tight-binding inhibitor as demonstrated by its K_i value. Compound 1 had a K_i value of 8.0 ± 0.1 nM. Eight concentrations of compound 1 were tested in order to determine K_i. This value is comparable to K_i values for the other tested compounds such as compounds 2 and 6. This suggests that this compound binds tightly with cruzain more so than compounds 2 and 6 bind with cruzain. Interestingly, the most potent compound, 3, exhibited a fairly high K_i value of 46.9 nM ± 11.3 nM. The standard error is greater than 10%, so more trials are warranted to confirm this value. Another explanation is that this inhibitor is a potent, slow-binding inhibitor that does not bind

tightly. Instead, it may form a reversible covalent bond. Future studies and manipulation of Morrison equation can exact this information. The compound with the lowest K_i value is compound 4. This indicates that compound 4 binds very tightly to cruzain. Tight inhibition is desirable in this case since inhibition of cruzain results in *T. cruzi* death. The hydroxyl group must aid in this tight-binding since this is the only structural variant between this compound and that of compound 3. Compounds 3 and 4 must bind in contrasting manners, and the reason may be traced due to para-substitution on the aromatic ring. Compounds 1 and 6, structural variants, exhibited drastic differences in K_i values of 8.0±0.1 and 47.6±1.4 nM, respectively. These are directly proportional to their respective IC_{50} values of 45.9±4.1 and 217.1±45.2 nM. If a compound is less potent and acts on enzyme through tight-binding, then it is reasonable to hypothesize a corresponding high K_i value. Therefore, results for compound 6 suggest this is not a desirable inhibitor.

Mechanism of action for TSC against cruzain

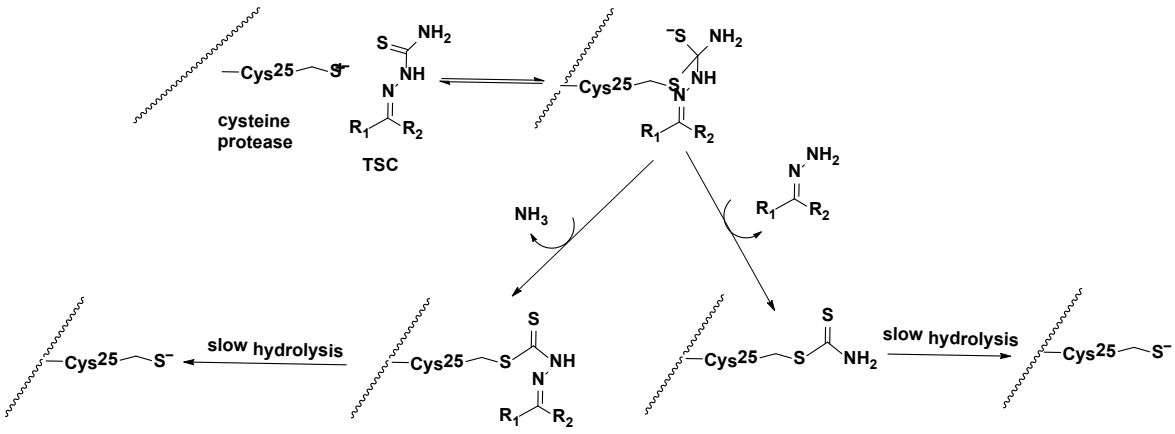

Figure 16. Proposed mechanism of inhibition for TSC derivatives against cruzain

The proposed mechanism, as illustrated in Figure 16, is similar to the mechanism of action of cruzipain. The mechanism of inhibition as proposed involves a nucleophilic attack of the thiolate anion of the cysteine residue that lines the region between the S1' and S1 pocket of the enzyme. The nearby residue stabilizes the tetrahedral intermediate formed from nucleophilic attack. Then, cleavage may occur in order to form a dithioamide. It slowly hydrolyzes to regenerate the active site. Results point to parts of this mechanism such as the attack of the thiocarbonyl. For example, functionalized compounds that allow for enhances electrophilicity of thiocarbonyl allows for a greater chance of nucleophilic attack by thiolate anions. Dibromobenzophenone analogs exhibited subnanomolar potency suggesting the benzophenone orients the thiocarbonyl of compounds near the nucleophilic cysteine. Regardless, this mechanism cannot be fully corroborated without further advanced kinetic studies.

Future studies

Future studies are warranted, especially for compound 1, in order to confirm this mode of inhibition. In order to ascertain reversibility, an excess of compound is incubated with cruzain for 4 h. The reaction is then diluted 100-fold to decrease the concentration of inhibitor ≤10% of its IC_{50} value for that preincubation time by the addition of 15 μM Z-FR-AMC solution to initiate the reaction. The reaction is followed for 2 additional hours. The recovery of cruzain activity as determined by the slope of the curve (change in AMC production as a function of time, μM/min) is most easily observed within the first couple of seconds of the reaction with substrate.

Also, obtaining an IC_{50} for longer preincubation times could elucidate how long it takes each compound to bind completely. Afterwards, advanced kinetic studies investigating the nature of equilibrium for each compound can elucidate is a compound is quickly reversible or slowly reversible. Then, IC_{50} values for varying concentrations of substrate can be determined in order to determine if inhibitors are competitive or not. Molecular modeling can be done in order to confirm mechanism of inhibition. In addition, these compounds can be evaluated against other mammalian cysteine proteases such as cathepsin L, homologous to cruzain, in order to assess compound specificity. After kinetic evaluation of inhibitors, the most potent compounds will advance to in vitro studies in order to assess antitrypanosomal properties. Murine or canine models are the next step before clinical trials.

Conclusion

From the series of TSC derivatives, synthesized by Dr. Kevin G. Pinney's laboratory, only compounds 1-6 demonstrated nanomolar potency. Compounds 1-3 were

confirmed to be potent time-dependent slowly binding inhibitors. Compound 1,2,4, and 6 were demonstrated to be tight-binding inhibitors while compound 3 is suggested to bind in some other fashion. In particular, compounds 1, 3, and 4 should be further explored for competitiveness, reversibility, and binding since these have demonstrated subnanomolar potency.

APPENDIX

APPENDIX A

Percent Inhibition with 5 minute preincubation time

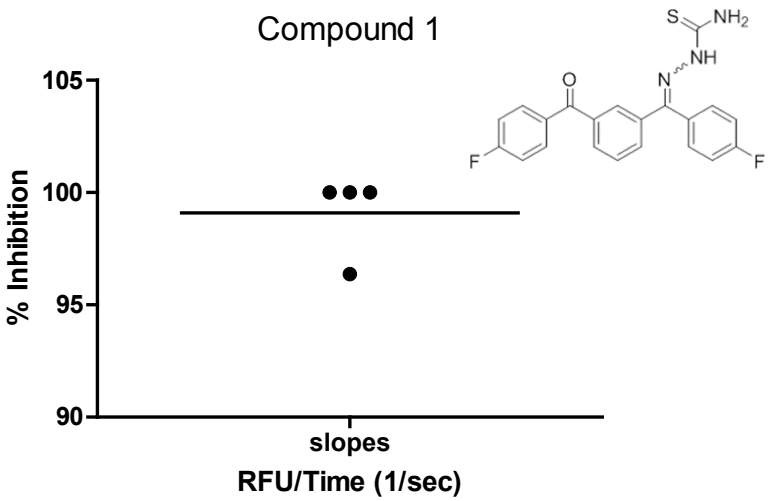

Figure 17.Percent inhibition of compound 1

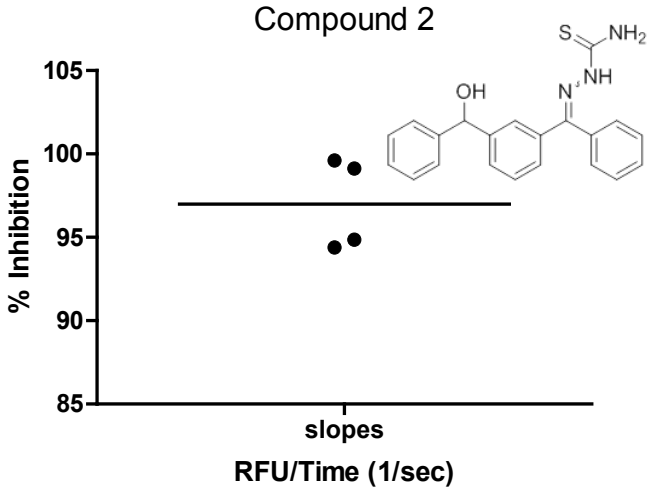

Figure 18.Percent inhibition of compound 2

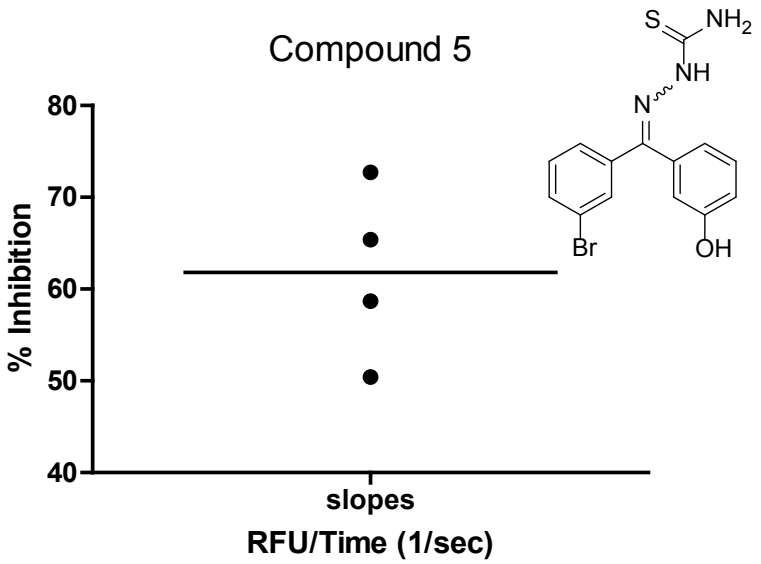

Figure 19. Percent inhibition of compound 5

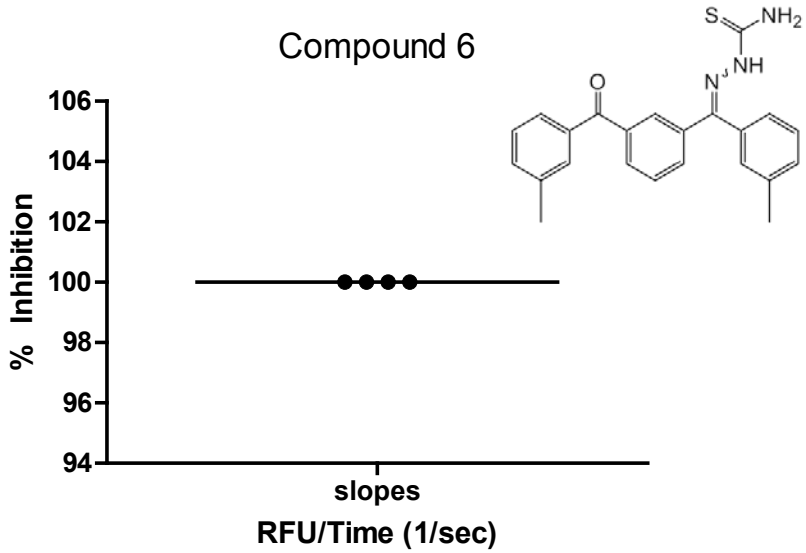

Figure 20.Percent inhibition of compound 6

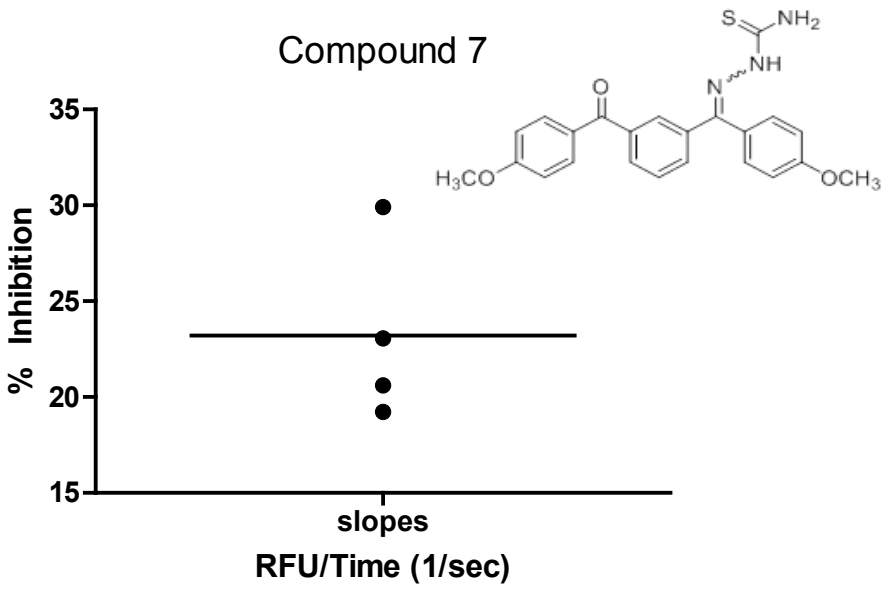

Figure 21.Percent inhibition of compound 7

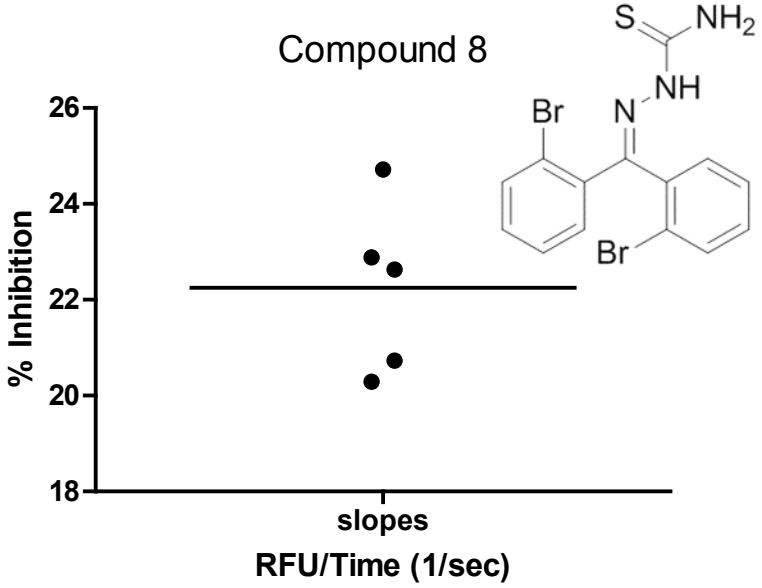

Figure 22.Percent inhibition of compound 8

APPENDIX B

Cruzain IC_{50} Determination Data and Plots

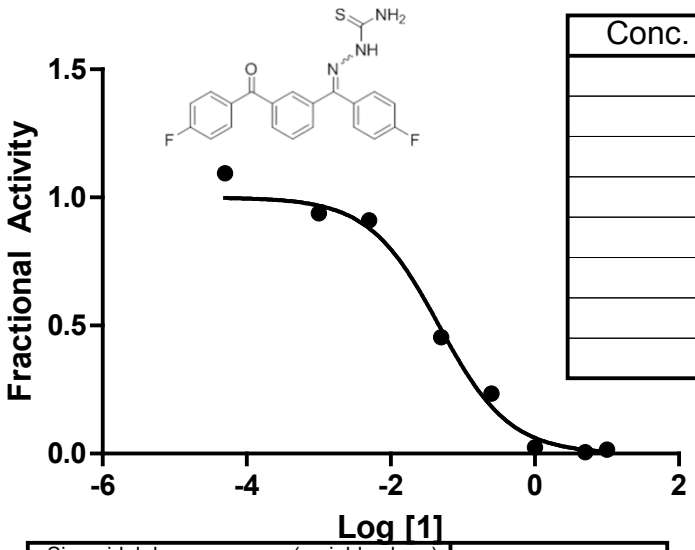

Conc. (μM)	slopes
1.000	0.015
0.699	0.005
0.000	0.024
-0.602	0.234
-1.301	0.455
-2.301	0.910
-3.000	0.938
-4.301	1.094

Sigmoidal dose-response (variable slope)	
Best-fit values	
Bottom	= 0.0
Top	= 1.000
LogEC50	-1.329
HillSlope	-0.8891
EC50	0.04692
Std. Error	
LogEC50	0.08133
HillSlope	0.1274
95% Confidence Intervals	
LogEC50	-1.528 to -1.130
HillSlope	-1.201 to -0.5775
EC50	0.02967 to 0.07419
Goodness of Fit	
Degrees of Freedom	6
R square	0.9891
Absolute Sum of Squares	0.01617
Sy.x	0.05191
Constraints	
Bottom	Bottom = 0.0
Top	Top = 1.000
Number of points	
Analyzed	8

Figure 23.Representative IC_{50} of Compound 1 with 5 minute preincubation time

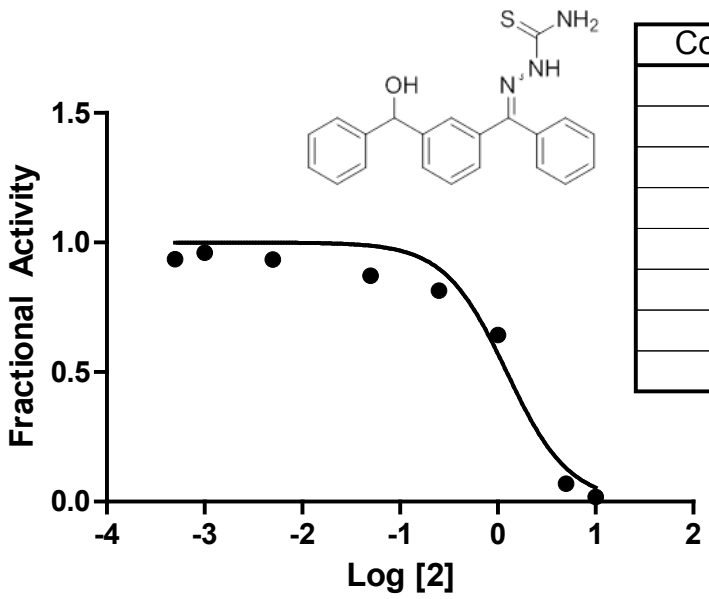

Conc. (μM)	slopes
1.000	0.018
0.699	0.069
0.000	0.644
-0.602	0.814
-1.301	0.871
-2.301	0.935
-3.000	0.960
-3.301	0.936

Sigmoidal dose-response (variable slope)	
Best-fit values	
Bottom	= 0.0
Top	= 1.000
LogEC50	0.09125
HillSlope	-1.364
EC50	1.234
Std. Error	
LogEC50	0.09058
HillSlope	0.3312
95% Confidence Intervals	
LogEC50	-0.1304 to 0.3129
HillSlope	-2.175 to -0.5538
EC50	0.7406 to 2.055
Goodness of Fit	
Degrees of Freedom	6
R square	0.9621
Absolute Sum of Squares	0.04062
Sy.x	0.08228
Constraints	
Bottom	Bottom = 0.0
Top	Top = 1.000
Number of points	
Analyzed	8

Figure 24.Representative IC_{50} of Compound 2 with 5 minute preincubation time

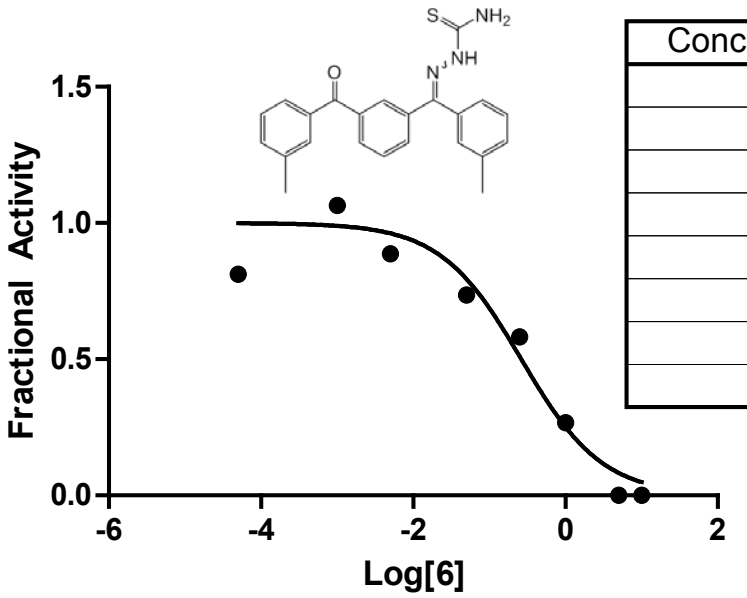

Conc. (μM)	slopes
1.000	0.0005
0.699	0.0000
0.000	0.2666
-0.602	0.5816
-1.301	0.7351
-2.301	0.8872
-3.000	1.0649
-4.301	0.8115

Sigmoidal dose-response (variable slope)	
Best-fit values	
Bottom	= 0.0
Top	= 1.000
LogEC50	-0.5794
HillSlope	-0.8154
EC50	0.2634
Std. Error	
LogEC50	0.1518
HillSlope	0.2129
95% Confidence Intervals	
LogEC50	-0.9508 to -0.2079
HillSlope	-1.336 to -0.2946
EC50	0.1120 to 0.6196
Goodness of Fit	
Degrees of Freedom	6
R square	0.9447
Absolute Sum of Squares	0.06457
Sy.x	0.1037
Constraints	
Bottom	Bottom = 0.0
Top	Top = 1.000
Number of points	
Analyzed	8

Figure 25.Representative of IC_{50} of Compound 6 with 5 minute preincubation time

APPENDIX C

Progress Curves

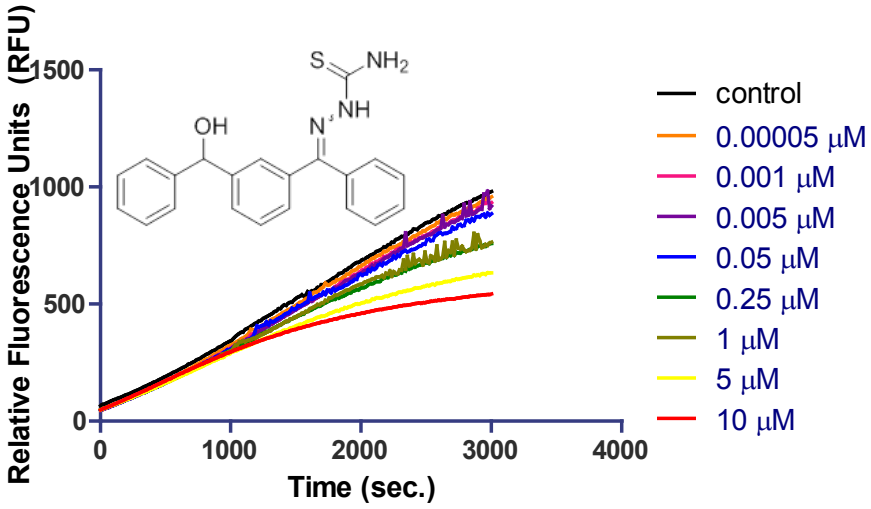

Figure 26.Representative of IC_{50} of Compound 2 with 5 minute preincubation time

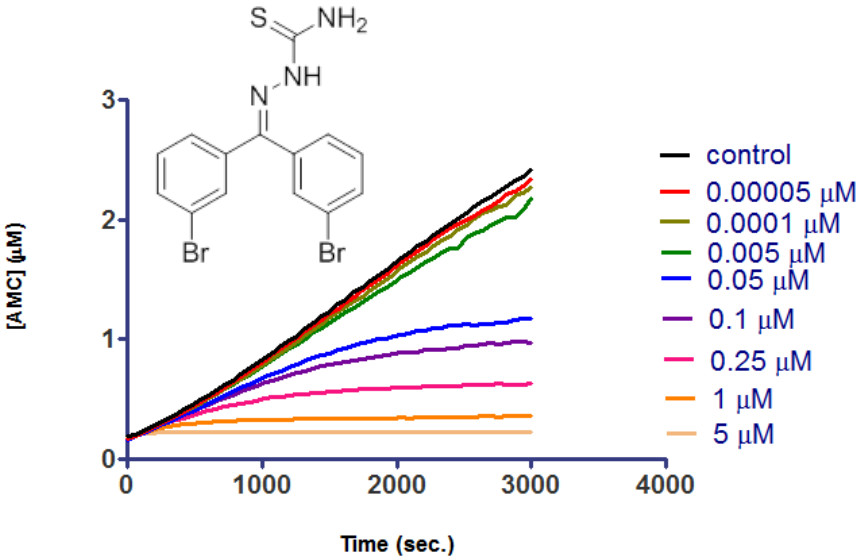

Figure 27.Representative of IC_{50} of Compound 3 with 5 minute preincubation time

APPENDIX D

Determination of K_i

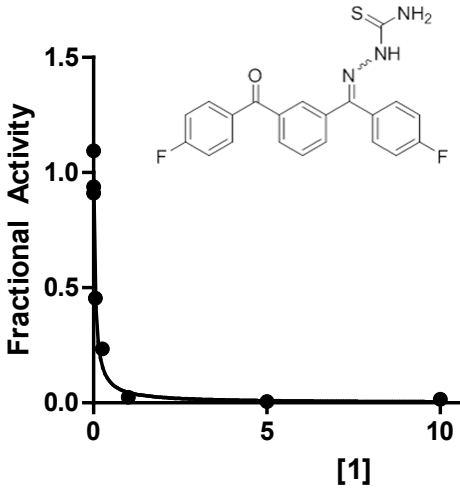

Morrison Ki	
Best-fit values	
Vo	= 1.000
Et	= 1.000e-005
Ki	0.007989
S	= 15.00
Km	= 3.000
Std. Error	
Ki	0.001348
95% Confidence Intervals	
Ki	0.004802 to 0.01118
Goodness of Fit	
Degrees of Freedom	7
R square	0.9878
Absolute Sum of Squares	0.01801
Sy.x	0.05072
Constraints	
Vo	Vo = 1.000
Et	Et = 1.000e-005
S	S = 15.00
Km	Km = 3.000
Number of points	
Analyzed	8

Figure 28.Graphical representation of Morrison equation for compound 1

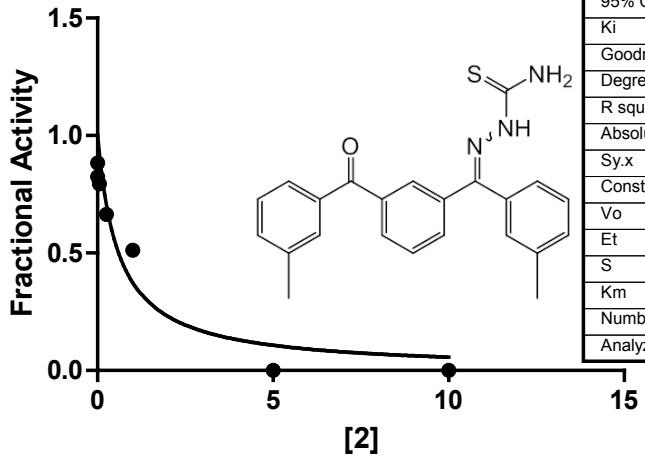

Morrison Ki	
Best-fit values	
Vo	= 1.000
Et	= 5.000e-005
Ki	0.1001
S	= 15.00
Km	= 3.000
Std. Error	
Ki	0.03701
95% Confidence Intervals	
Ki	0.009524 to 0.1907
Goodness of Fit	
Degrees of Freedom	6
R square	0.8903
Absolute Sum of Squares	0.09446
Sy.x	0.1255
Constraints	
Vo	Vo = 1.000
Et	Et = 5.000e-005
S	S = 15.00
Km	Km = 3.000
Number of points	
Analyzed	7

Figure 29.Graphical representation of Morrison equation for compound 2

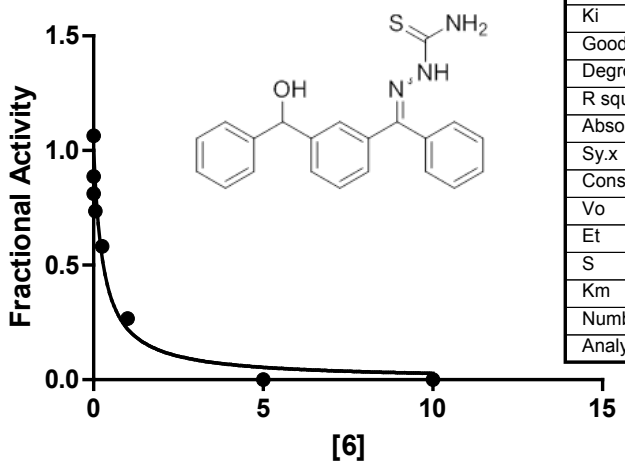

Morrison Ki	
Best-fit values	
Vo	= 1.000
Et	= 5.000e-005
Ki	0.04765
S	= 15.00
Km	= 3.000
Std. Error	
Ki	0.01434
95% Confidence Intervals	
Ki	0.01374 to 0.08157
Goodness of Fit	
Degrees of Freedom	7
R square	0.9394
Absolute Sum of Squares	0.07069
Sy.x	0.1005
Constraints	
Vo	Vo = 1.000
Et	Et = 5.000e-005
S	S = 15.00
Km	Km = 3.000
Number of points	
Analyzed	8

Figure 30.Graphical representation of Morrison equation for compound 6

APPENDIX E

Preincubation graphs with respective cruzain IC_{50} determination data and plots

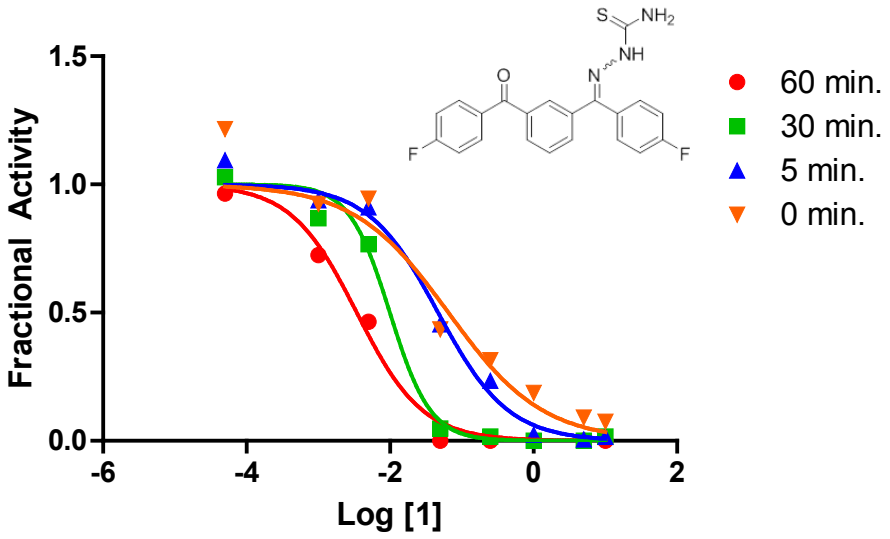

Figure 31.Preincubation graph with respective cruzain IC50 determination plots for compound 1

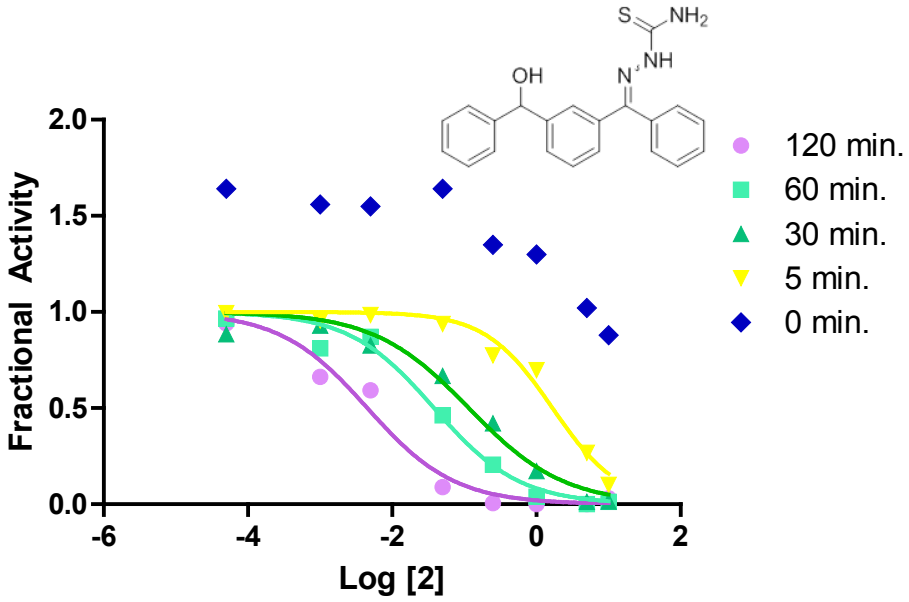

Figure 32.Preincubation graph with respective cruzain IC_{50} determination plots for compound 2

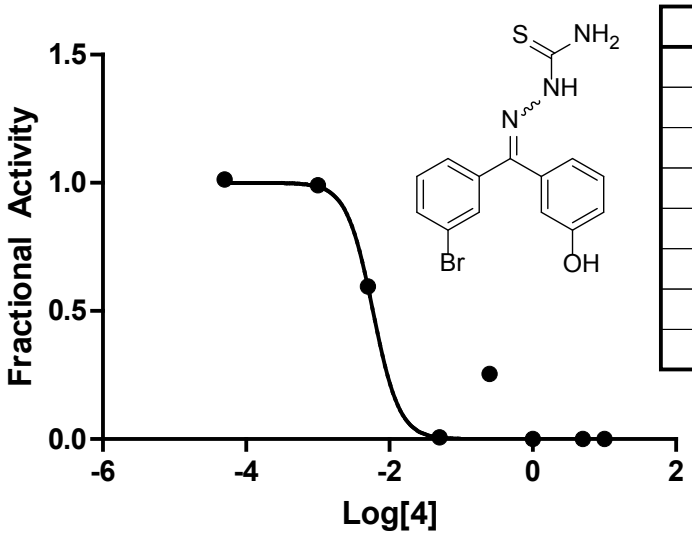

Conc. (μM)	slopes
1.000	0.000
0.699	0.000
0.000	0.000
-0.602	0.254
-1.301	0.006
-2.301	0.596
-3.000	0.991
-4.301	1.013

Sigmoidal dose-response (variable slope)	
Best-fit values	
Bottom	= 0.0
Top	= 1.000
LogEC50	-2.229
HillSlope	-2.359
EC50	0.005897
Std. Error	
LogEC50	0.1408
HillSlope	3.730
95% Confidence Intervals	
LogEC50	-2.574 to -1.885
HillSlope	-11.49 to 6.769
EC50	0.002667 to 0.01304
Goodness of Fit	
Degrees of Freedom	6
R square	0.9538
Absolute Sum of Squares	0.06489
Sy.x	0.1040
Constraints	
Bottom	Bottom = 0.0
Top	Top = 1.000
Number of points	
Analyzed	8

Figure 33.Representative of IC_{50} determination plots for compound 4 with preincubation time of 30 minutes

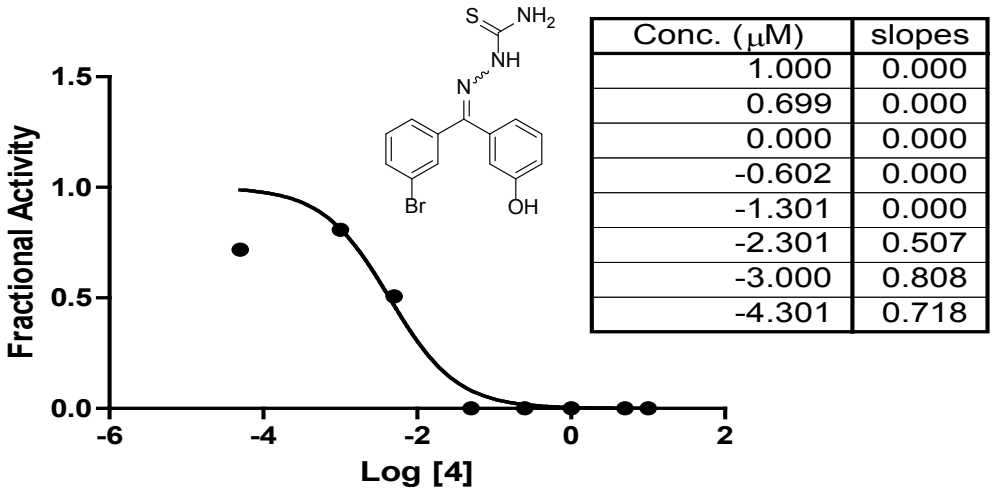

Conc. (μM)	slopes
1.000	0.000
0.699	0.000
0.000	0.000
-0.602	0.000
-1.301	0.000
-2.301	0.507
-3.000	0.808
-4.301	0.718

Sigmoidal dose-response (variable slope)	
Best-fit values	
Bottom	= 0.0
Top	= 1.000
LogEC50	-2.360
HillSlope	-0.9941
EC50	0.004368
Std. Error	
LogEC50	0.1699
HillSlope	0.3852
95% Confidence Intervals	
LogEC50	-2.776 to -1.944
HillSlope	-1.937 to -0.05159
EC50	0.001677 to 0.01138
Goodness of Fit	
Degrees of Freedom	6
R square	0.9104
Absolute Sum of Squares	0.08151
Sy.x	0.1166
Constraints	
Bottom	Bottom = 0.0
Top	Top = 1.000
Number of points	
Analyzed	8

Figure 34.Representative of IC_{50} determination plots for compound 4 with preincubation time of 60 minutes

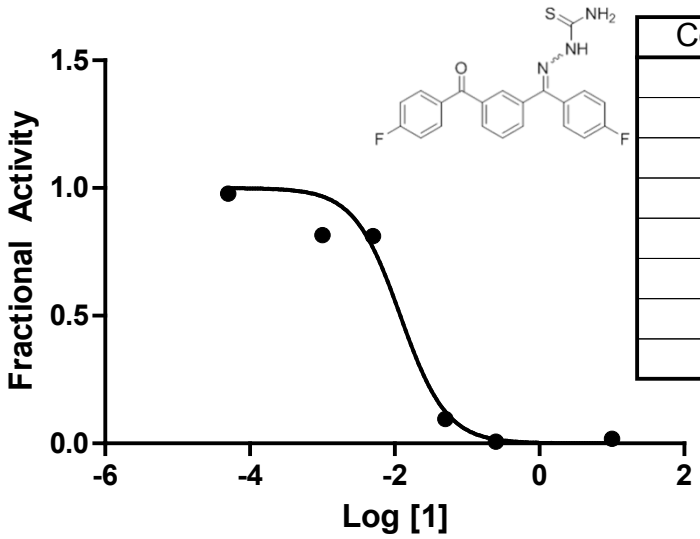

Conc. (μM)	slopes
1.000	0.0185
0.699	
0.000	
-0.602	0.0074
-1.301	0.0959
-2.301	0.8120
-3.000	0.8162
-4.301	0.9776

Sigmoidal dose-response (variable slope)	
Best-fit values	
Bottom	= 0.0
Top	= 1.000
LogEC50	-1.922
HillSlope	-1.362
EC50	0.01197
Std. Error	
LogEC50	0.1262
HillSlope	0.3516
95% Confidence Intervals	
LogEC50	-2.272 to -1.571
HillSlope	-2.338 to -0.3862
EC50	0.005346 to 0.02682
Goodness of Fit	
Degrees of Freedom	4
R square	0.9747
Absolute Sum of Squares	0.02655
Sy.x	0.08148
Constraints	
Bottom	Bottom = 0.0
Top	Top = 1.000
Number of points	
Analyzed	6

Figure 35.Representative of IC_{50} determination plots for compound 1 with preincubation time of 30 minutes

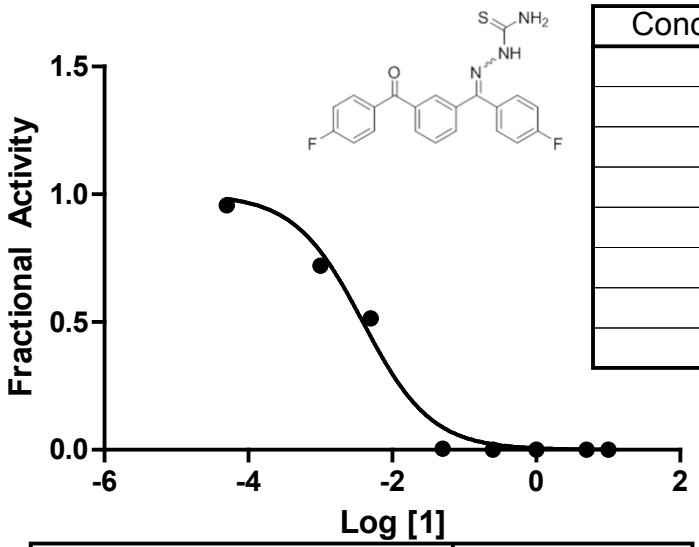

Conc. (μM)	slopes
1.000	0.000
0.699	0.000
0.000	0.000
-0.602	0.000
-1.301	0.004
-2.301	0.515
-3.000	0.721
-4.301	0.957

Sigmoidal dose-response (variable slope)	
Best-fit values	
Bottom	= 0.0
Top	= 1.000
LogEC50	-2.408
HillSlope	-0.9149
EC50	0.003906
Std. Error	
LogEC50	0.07941
HillSlope	0.1533
95% Confidence Intervals	
LogEC50	-2.603 to -2.214
HillSlope	-1.290 to -0.5397
EC50	0.002497 to 0.006110
Goodness of Fit	
Degrees of Freedom	6
R square	0.9850
Absolute Sum of Squares	0.01640
Sy.x	0.05229
Constraints	
Bottom	Bottom = 0.0
Top	Top = 1.000
Number of points	
Analyzed	8

Figure 36.Representative of IC_{50} determination plots for compound 1 with preincubation time of 60 minutes

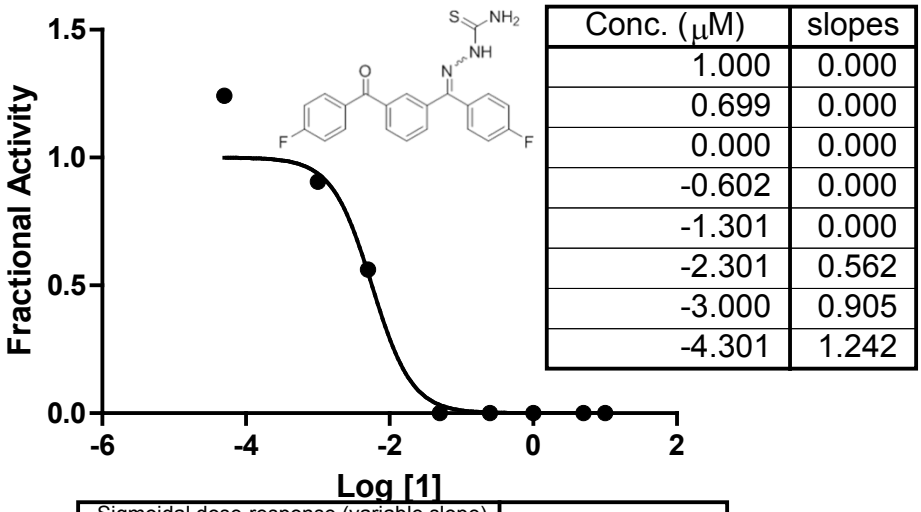

Conc. (μM)	slopes
1.000	0.000
0.699	0.000
0.000	0.000
-0.602	0.000
-1.301	0.000
-2.301	0.562
-3.000	0.905
-4.301	1.242

Sigmoidal dose-response (variable slope)	
Best-fit values	
Bottom	= 0.0
Top	= 1.000
LogEC50	-2.245
HillSlope	-1.562
EC50	0.005690
Std. Error	
LogEC50	0.1171
HillSlope	0.8516
95% Confidence Intervals	
LogEC50	-2.532 to -1.958
HillSlope	-3.646 to 0.5223
EC50	0.002941 to 0.01101
Goodness of Fit	
Degrees of Freedom	6
R square	0.9654
Absolute Sum of Squares	0.06088
Sy.x	0.1007
Constraints	
Bottom	Bottom = 0.0
Top	Top = 1.000
Number of points	
Analyzed	8

Figure 37.Representative of IC_{50} determination plots for compound 1 with preincubation time of 120 minutes

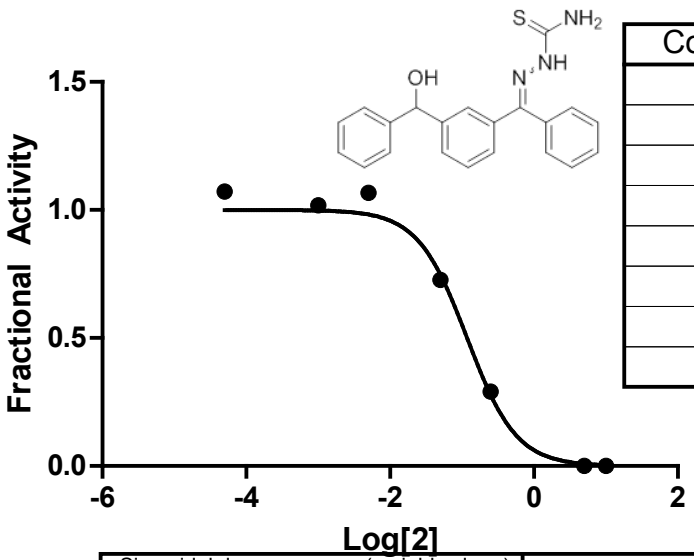

Conc. (μM)	slopes
1.000	0.000
0.699	0.000
0.000	
-0.602	0.291
-1.301	0.727
-2.301	1.067
-3.000	1.018
-4.301	1.071

Sigmoidal dose-response (variable slope)	
Best-fit values	
Bottom	= 0.0
Top	= 1.000
LogEC50	-0.9283
HillSlope	-1.268
EC50	0.1180
Std. Error	
LogEC50	0.06418
HillSlope	0.2239
95% Confidence Intervals	
LogEC50	-1.093 to -0.7633
HillSlope	-1.843 to -0.6921
EC50	0.08068 to 0.1725
Goodness of Fit	
Degrees of Freedom	5
R square	0.9907
Absolute Sum of Squares	0.01338
Sy.x	0.05174
Constraints	
Bottom	Bottom = 0.0
Top	Top = 1.000
Number of points	
Analyzed	7

Figure 38.Representative of IC_{50} determination plots for compound 2 with preincubation time of 30 minutes

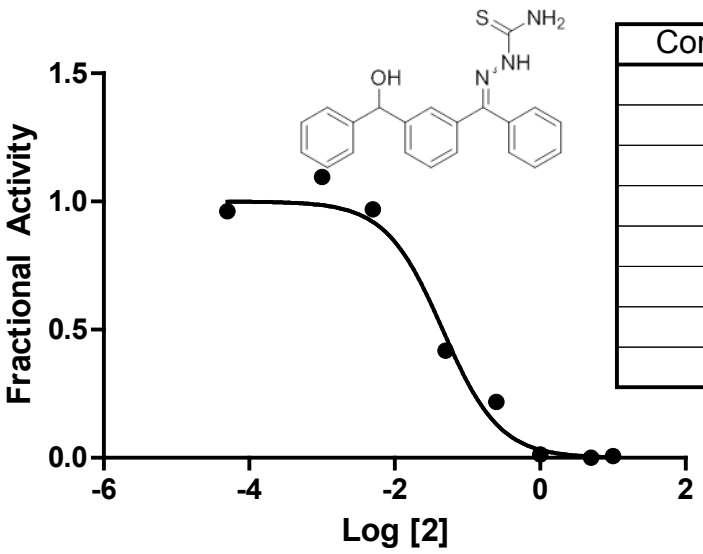

Conc. (μM)	slopes
1.000	0.007
0.699	0.000
0.000	0.013
-0.602	0.218
-1.301	0.418
-2.301	0.970
-3.000	1.095
-4.301	0.962

Sigmoidal dose-response (variable slope)	
Best-fit values	
Bottom	= 0.0
Top	= 1.000
LogEC50	-1.339
HillSlope	-1.108
EC50	0.04577
Std. Error	
LogEC50	0.09432
HillSlope	0.2478
95% Confidence Intervals	
LogEC50	-1.570 to -1.109
HillSlope	-1.714 to -0.5018
EC50	0.02690 to 0.07787
Goodness of Fit	
Degrees of Freedom	6
R square	0.9831
Absolute Sum of Squares	0.02692
Sy.x	0.06698
Constraints	
Bottom	Bottom = 0.0
Top	Top = 1.000
Number of points	
Analyzed	8

Figure 39.Representative of IC_{50} determination plots for compound 2 with preincubation time of 60 minutes

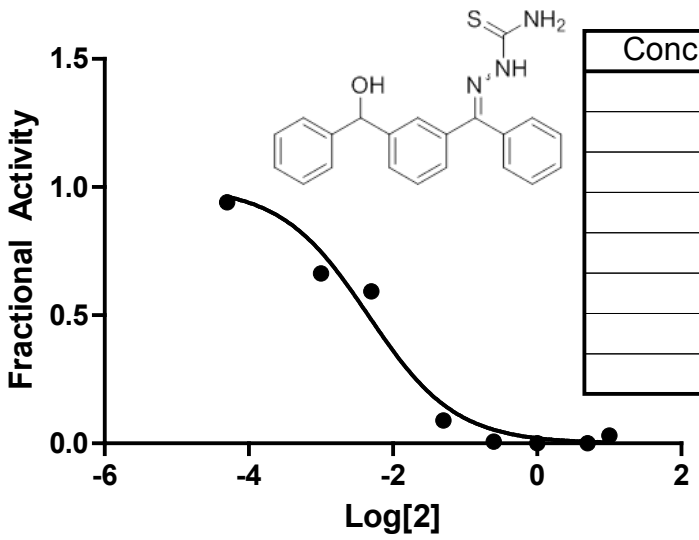

Conc. (μM)	slopes
1.000	0.031
0.699	0.000
0.000	0.000
-0.602	0.006
-1.301	0.090
-2.301	0.593
-3.000	0.663
-4.301	0.941

Sigmoidal dose-response (variable slope)	
Best-fit values	
Bottom	= 0.0
Top	= 1.000
LogEC50	-2.343
HillSlope	-0.7175
EC50	0.004542
Std. Error	
LogEC50	0.1175
HillSlope	0.1312
95% Confidence Intervals	
LogEC50	-2.630 to -2.055
HillSlope	-1.039 to -0.3964
EC50	0.002343 to 0.008806
Goodness of Fit	
Degrees of Freedom	6
R square	0.9734
Absolute Sum of Squares	0.02687
Sy.x	0.06693
Constraints	
Bottom	Bottom = 0.0
Top	Top = 1.000
Number of points	
Analyzed	8

Figure 40.Representative of IC_{50} determination plots for compound 2 with preincubation time of 120 minutes

REFERENCES

(1) Montgomery, S. P.; Starr, M. C.; Cantey, P. T.; Edwards, M. S.; Meymandi, S. K. Neglected Parasitic Infections in the United States: Chagas Disease. *Am. J. Trop. Med. Hyg.* **2014**, *90* (5), 814–818.

(2) Martins-Melo, F. R.; Ramos, A. N.; Alencar, C. H.; Heukelbach, J. Prevalence of Chagas Disease in Brazil: A Systematic Review and Meta-Analysis. *Acta Trop.* **2014**, *130*, 167–174.

(3) Miró, J. M.; Blanes, M.; Norman, F.; Martín-Dávila, P. Infections in Solid Organ Transplantation in Special Situations: HIV-Infection and Immigration. *Enferm. Infecc. Microbiol. Clin.* **2012**, *30 Suppl 2*, 76–85.

(4) Cantey, P. T.; Stramer, S. L.; Townsend, R. L.; Kamel, H.; Ofafa, K.; Todd, C. W.; Currier, M.; Hand, S.; Varnado, W.; Dotson, E.; Hall, C.; Jett, P. L.; Montgomery, S. P. The United States Trypanosoma Cruzi Infection Study: Evidence for Vector-Borne Transmission of the Parasite That Causes Chagas Disease among United States Blood Donors. *Transfusion* **2012**, *52* (9), 1922–1930.

(5) Nunes, M. C. P.; Dones, W.; Morillo, C. A.; Encina, J. J.; Ribeiro, A. L. Chagas Disease: An Overview of Clinical and Epidemiological Aspects. *Journal of the American College of Cardiology*. 2013, pp 767–776.

(6) Bern, C.; Montgomery, S. P.; Herwaldt, B. L.; Marin-neto, J. A.; Maguire, J. H.; Acquatella, H.; Morillo, C.; Gilman, R. H.; Reyes, P. A.; Salvatella, R. CLINICIAN ' S CORNER Evaluation and Treatment of Chagas Disease in the United States A Systematic Review. **2007**, *298* (18), 2171–2181.

(7) Hotez, P. J.; Dumonteil, E.; Betancourt Cravioto, M.; Bottazzi, M. E.; Tapia-Conyer, R.; Meymandi, S.; Karunakara, U.; Ribeiro, I.; Cohen, R. M.; Pecoul, B. An Unfolding Tragedy of Chagas Disease in North America. *PLoS Negl. Trop. Dis.* **2013**, *7* (10), e2300.

(8) Tyler, K.; Olson, C.; Engman, D. The Life Cycle Of Trypanosoma Cruzi. In *American Trypanosomiasis*; 2002; Vol. 7, pp 1–11.

(9) Goldenberg, S.; Avila, A. R. Aspects of Trypanosoma Cruzi Stage Differentiation. *Adv. Parasitol.* **2011**, *75*, 285–305.

(10) Jackson, Y.; Getaz, L.; Wolff H., Holst M.;Mauris, A. Prevalence, Clinical Staging and Risk for Blood-Borne Transmission of Chagas' Disease among Latin American Migrants. *PLoS Negl Trop Dis* **2010**, *2* (4), e597.

(11) Scharfstein, J.; Andrade, D. Infection-Associated Vasculopathy in Experimental Chagas Disease Pathogenic Roles of Endothelin and Kinin Pathways. *Adv. Parasitol.* **2011**, *76*, 101–127.

(12) Urbina, J. A. Specific Chemotherapy of Chagas Disease: Relevance, Current Limitations and New Approaches. *Acta Trop.* **2010**, *115* (1-2), 55–68.

(13) Urbina, J. A. Recent Clinical Trials for the Etiological Treatment of Chronic Chagas Disease: Advances, Challenges and Perspectives. *Journal of Eukaryotic Microbiology*. 2015, pp 149–156.

(14) Hall, B. S.; Wilkinson, S. R. Activation of Benznidazole by Trypanosomal Type I Nitroreductases Results in Glyoxal Formation. *Antimicrob. Agents Chemother.* **2012**, *56* (1), 115–123.

(15) Castro, J. a; de Mecca, M. M.; Bartel, L. C. Toxic Side Effects of Drugs Used to Treat Chagas' Disease (American Trypanosomiasis). *Hum. Exp. Toxicol.* **2006**, *25* (8), 471–479.

(16) Molina, I.; Gómez i Prat, J.; Salvador, F.; Treviño, B.; Sulleiro, E.; Serre, N.; Pou, D.; Roure, S.; Cabezos, J.; Valerio, L.; Blanco-Grau, A.; Sánchez-Montalvá, A.; Vidal, X.; Pahissa, A. Randomized Trial of Posaconazole and Benznidazole for Chronic Chagas' Disease. *N. Engl. J. Med.* **2014**, *370* (20), 1899–1908.

(17) Sajid, M.; Robertson, S. A.; Brinen, L. S.; McKerrow, J. H. Cruzain : The Path from Target Validation to the Clinic. *Adv. Exp. Med. Biol.* **2011**, *712*, 100–115.

(18) Pham, J. S.; Dawson, K. L.; Jackson, K. E.; Lim, E. E.; Pasaje, C. F. A.; Turner, K. E. C.; Ralph, S. A. Aminoacyl-tRNA Synthetases as Drug Targets in Eukaryotic Parasites. *Int. J. Parasitol. Drugs drug Resist.* **2014**, *4* (1), 1–13.

(19) Hoekstra, W.J.;Hargrove, T.Y.;Wawrzak, Z.;de Gama Jaen Batista, D.;da Silva, C.F.;Nefertiti, A.S.G;Schotzinger, R.J.;Villalta, F.;de Nazaré C.Soeiro, M.;Lepesheva, G. I. Clinical Candidate VT-1161's Antiparasitic Effect In Vitro, Activity in a Murine Model of Chagas Disease, and Structural Characterization in Complex with the Target Enzyme CYP51 from Trypanosoma Cruzi. *Antimicrob. Agents Chemother.* **2015**, No. 60, 1058–1066.

(20) Villalta, F.; Dobish, M. C.; Nde, P. N.; Kleshchenko, Y. Y.; Hargrove, T. Y.; Johnson, C. A.; Waterman, M. R.; Johnston, J. N.; Lepesheva, G. I. VNI Cures Acute and Chronic Experimental Chagas Disease. *J. Infect. Dis.* **2013**, *208* (3), 504–511.

(21) Cazzulo, J. J.; Niemirowicz, G. T.; Frasch, A. P.; José Cazzulo, J.; Myburgh, E.; Coombs, G. H.; Mottram, J. C. *Handbook of Proteolytic Enzymes*; Elsevier, 2013.

(22) Polticelli, Fabio; Zaini, Germano; Boli, Allesandro; Antonini, Giovanni; Gradoni, Luigi; Ascenzi, P. Probing the Cruzain S2 Recognition Subsite- A Kinetic and Binding Energy Calculation Study. *Biochemistry* **2005**, No. 44, 2781–2789.

(23) Otto, H.-H.; Schirmeister, T. Cysteine Proteases and Their Inhibitors. *Chem. Rev.* **1997**, *97* (1), 133–172.

(24) Lee, G. M.; Balouch, E.; Goetz, D. H.; Lazic, a; McKerrow, J. H.; Craik, C. S.

Mapping Inhibitor Binding Modes on an Active Cysteine Protease via NMR Spectroscopy. *Biochemistry* **2012**.

(25) Greenbaum, D. C.; Mackey, Z.; Hansell, E.; Doyle, P.; Gut, J.; Caffrey, C. R.; Lehrman, J.; Rosenthal, P. J.; McKerrow, J. H.; Chibale, K. Synthesis and Structure-Activity Relationships of Parasiticidal Thiosemicarbazone Cysteine Protease Inhibitors against Plasmodium Falciparum, Trypanosoma Brucei, and Trypanosoma Cruzi. *J. Med. Chem.* **2004**, *47* (12), 3212–3219.

(26) Maeda, F. Y.; Cortez, C.; Yoshida, N. Cell Signaling during Trypanosoma Cruzi Invasion. *Front. Immunol.* **2012**, *3*, 1–7.

(27) Epting, C. L.; Coates, B. M.; Engman, D. M. Molecular Mechanisms of Host Cell Invasion by Trypanosoma Cruzi. *Exp. Parasitol.* **2010**, *126* (3), 283–291.

(28) Chen, S.-E. Modeling, Design, and Development of Potential Inhibitors of Y-Glutamylamine Cyclotransferase and Inhibitors of Cruzain as Therapeutic Agentgs for Chagas' Disease., Baylor University, 2008.

(29) de Oliveira Filho, G. B.; de Oliveira Cardoso, M. V.; Espíndola, J. W. P.; Ferreira, L. F. G. R.; de Simone, C. A.; Ferreira, R. S.; Coelho, P. L.; Meira, C. S.; Magalhaes Moreira, D. R.; Soares, M. B. P.; Lima Leite, A. C. Structural Design, Synthesis and Pharmacological Evaluation of 4-Thiazolidinones against Trypanosoma Cruzi. *Bioorg. Med. Chem.* **2015**, *23* (23), 7478–7486.

(30) Carvalho, S. A.; Feitosa, L. O.; Soares, M.; Costa, T. E. M. M.; Henriques, M. G.; Salomão, K.; de Castro, S. L.; Kaiser, M.; Brun, R.; Wardell, J. L.; Wardell, S. M. S. V; Trossini, G. H. G.; Andricopulo, A. D.; da Silva, E. F.; Fraga, C. A. M. Design and Synthesis of New (E)-Cinnamic N-Acylhydrazones as Potent Antitrypanosomal Agents. *Eur. J. Med. Chem.* **2012**, *54*, 512–521.

(31) Bellera, C. L.; Balcazar, D. E.; Alberca, L.; Labriola, C. A.; Talevi, A.; Carrillo, C. Identification of Levothyroxine Antichagasic Activity through Computer-Aided Drug Repurposing. *Sci. World J.* **2014**, *2014*, 1–10.

(32) Ndao, M.; Beaulieu, C.; Black, W. C.; Isabel, E.; Vasquez-Camargo, F.; Nath-Chowdhury, M.; Mass??, F.; Mellon, C.; Methot, N.; Nicoll-Griffith, D. A. Reversible Cysteine Protease Inhibitors Show Promise for a Chagas Disease Cure. *Antimicrob. Agents Chemother.* **2014**, *58* (2), 1167–1178.

(33) Borchhardt, D. M.; Mascarello, A.; Chiaradia, L. D.; Nunes, R. J.; Oliva, G.; Yunes, R. A.; Andricopulo, A. D. Biochemical Evaluation of a Series of Synthetic Chalcone and Hydrazide Derivatives as Novel Inhibitors of Cruzain from Trypanosoma Cruzi. *J. Braz. Chem. Soc.* **2010**.

(34) Dunny, E.; Evans, P. Vinyl Sulfone Containing Parasitic Cysteinyl Protease Inhibitors. *Curr. Bioact. Compd.* **2011**, *7* (4), 218–236.

(35) Bellera, C. L.; Balcazar, D. E.; Vanrell, M. C.; Casassa, A. F.; Palestro, P. H.;

Gavernet, L.; Labriola, C. A.; Gálvez, J.; Bruno-Blanch, L. E.; Romano, P. S.; Carrillo, C.; Talevi, A. Computer-Guided Drug Repurposing: Identification of Trypanocidal Activity of Clofazimine, Benidipine and Saquinavir. *Eur. J. Med. Chem.* **2015**, *93*, 338–348.

(36) Ferreira, R. S.; Simeonov, A.; Jadhav, A.; Eidam, O.; Mott, B. T.; Keiser, M. J.; McKerrow, J. H.; Maloney, D. J.; Irwin, J. J.; Shoichet, B. K. Complementarity between a Docking and a High-Throughput Screen in Discovering New Cruzain Inhibitors. *J. Med. Chem.* **2010**, *53* (13), 4891–4905.

(37) Monteiro, a C.; Abrahamson, M.; Lima, a P.; Vannier-Santos, M. a; Scharfstein, J. Identification, Characterization and Localization of Chagasin, a Tight-Binding Cysteine Protease Inhibitor in Trypanosoma Cruzi. *J. Cell Sci.* **2001**, *114* (Pt 21), 3933–3942.

(38) Buarque, D. S.; Spindola, L. M. N.; Martins, R. M.; Braz, G. R. C.; Tanaka, A. S. Tigutcystatin, a Cysteine Protease Inhibitor from Triatoma Infestans Midgut Expressed in Response to Trypanosoma Cruzi. *Biochem. Biophys. Res. Commun.* **2011**, *413* (2), 241–247.

(39) Castro, H. C.; Abreu, P. A.; Geraldo, R. B.; Martins, R. C. A.; dos Santos, R.; Loureiro, N. I. V; Cabral, L. M.; Rodrigues, C. R. Looking at the Proteases from a Simple Perspective. *J. Mol. Recognit.* **2011**, *24* (2), 165–181.

(40) Choe, Y.; Brinen, L. S.; Price, M. S.; Engel, J. C.; Lange, M.; Grisostomi, C.; Weston, S. G.; Pallai, P. V; Cheng, H.; Hardy, L. W.; Hartsough, D. S.; McMakin, M.; Tilton, R. F.; Baldino, C. M.; Craik, C. S. Development of Alpha-Keto-Based Inhibitors of Cruzain, a Cysteine Protease Implicated in Chagas Disease. *Bioorg. Med. Chem.* **2005**, *13* (6), 2141–2156.

(41) Beaulieu, C.; Isabel, E.; Fortier, A.; Mass??, F.; Mellon, C.; M??thot, N.; Ndao, M.; Nicoll-Griffith, D.; Lee, D.; Park, H.; Black, W. C. Identification of Potent and Reversible Cruzipain Inhibitors for the Treatment of Chagas Disease. *Bioorganic Med. Chem. Lett.* **2010**, *20* (24), 7444–7449.

(42) Avelar, L. A. A.; Camilo, C. D.; de Albuquerque, S.; Fernandes, W. B.; Gonçalez, C.; Kenny, P. W.; Leitão, A.; McKerrow, J. H.; Montanari, C. A.; Orozco, E. V. M.; Ribeiro, J. F. R.; Rocha, J. R.; Rosini, F.; Saidel, M. E. Molecular Design, Synthesis and Trypanocidal Activity of Dipeptidyl Nitriles as Cruzain Inhibitors. *PLoS Negl. Trop. Dis.* **2015**, *9* (7), e0003916.

(43) Pizzo, C.; Saiz, C.; Talevi, A.; Gavernet, L.; Palestro, P.; Bellera, C.; Blanch, L. B.; Benítez, D.; Cazzulo, J. J.; Chidichimo, A.; Wipf, P.; Mahler, S. G. Synthesis of 2-Hydrazolyl-4-Thiazolidinones Based on Multicomponent Reactions and Biological Evaluation Against Trypanosoma Cruzi. *Chem. Biol. Drug Des.* **2011**.

(44) Song, J.; Jones, L. M.; Kumar, G. D. K.; Conner, E. S.; Bayeh, L.; Chavarria, G. E.; Charlton-Sevcik, A. K.; Chen, S. E.; Chaplin, D. J.; Trawick, M. L.; Pinney, K. G. Synthesis and Biochemical Evaluation of Thiochromanone Thiosemicarbazone

Analogues as Inhibitors of Cathepsin L. *ACS Med. Chem. Lett.* **2012**, *3*, 450–453.

(45) Song, J.; Jones, L. M.; Chavarria, G. E.; Charlton-Sevcik, A. K.; Jantz, A.; Johansen, A.; Bayeh, L.; Soeung, V.; Snyder, L. K.; Lade, S. D.; Chaplin, D. J.; Trawick, M. L.; Pinney, K. G. Small-Molecule Inhibitors of Cathepsin L Incorporating Functionalized Ring-Fused Molecular Frameworks. *Bioorganic Med. Chem. Lett.* **2013**, *23* (9), 2801–2807.

(46) Chavarria, G. E.; Horsman, M. R.; Arispe, W. M.; Kishore Kumar, G. D.; Chen, S. E.; Strecker, T. E.; Parker, E. N.; Chaplin, D. J.; Pinney, K. G.; Trawick, M. L. Initial Evaluation of the Antitumour Activity of KGP94, a Functionalized Benzophenone Thiosemicarbazone Inhibitor of Cathepsin L. *Eur. J. Med. Chem.* **2012**, *58*, 568–572.

(47) Fujii, N.; Mallari, J. P.; Hansell, E. J.; MacKey, Z.; Doyle, P.; Zhou, Y. M.; Gut, J.; Rosenthal, P. J.; McKerrow, J. H.; Guy, R. K. Discovery of Potent Thiosemicarbazone Inhibitors of Rhodesain and Cruzain. *Bioorganic Med. Chem. Lett.* **2005**, *15*, 121–123.

(48) Siles, R.; Chen, S.-E.; Zhou, M.; Pinney, K. G.; Trawick, M. L. Design, Synthesis, and Biochemical Evaluation of Novel Cruzain Inhibitors with Potential Application in the Treatment of Chagas' Disease. *Bioorg. Med. Chem. Lett.* **2006**, *16* (16), 4405–4409.

(49) Blau, L.; Menegon, R. F.; Trossini, G. H. G.; Molino, J. V. D.; Vital, D. G.; Cicarelli, R. M. B.; Passerini, G. D.; Bosquesi, P. L.; Chin, C. M. Design, Synthesis and Biological Evaluation of New Aryl Thiosemicarbazone as Antichagasic Candidates. *Eur. J. Med. Chem.* **2013**.

(50) Wanderlan Pontes Espíndola, J.; Veríssimo de Oliveira Cardoso, M.; Bezerra de Oliveira Filho, G.; Albuquerque Oliveira Silva, D.; Rodrigo Magalhaes Moreira, D.; Matutino Bastos, T.; Alberto de Simone, C.; Botelho Pereira Soares, M.; Silva Villela, F.; Salgado Ferreira, R.; Carolina Accioly Brelaz de Castro, M.; eria Rego Alves Pereira, V.; Maria Fonseca Murta, S.; Ademar Sales Junior, P.; Jos Romanha, A.; Cristina Lima Leite, A. Synthesis and Structure-Activity Relationship Study of a New Series of Antiparasitic Aryloxyl Thiosemicarbazones Inhibiting Trypanosoma Cruzi Cruzain. *Eur. J. Med. Chem.* **2015**, *101*, 818–835.

(51) Parker, E. N.; Song, J.; Kishore Kumar, G. D.; Odutola, S. O.; Chavarria, G. E.; Charlton-Sevcik, A. K.; Strecker, T. E.; Barnes, A. L.; Sudhan, D. R.; Wittenborn, T. R.; Siemann, D. W.; Horsman, M. R.; Chaplin, D. J.; Trawick, M. L.; Pinney, K. G. Synthesis and Biochemical Evaluation of Benzoylbenzophenone Thiosemicarbazone Analogues as Potent and Selective Inhibitors of Cathepsin L. *Bioorganic Med. Chem.* **2015**, *23* (21), 6974–6992.

(52) Song, J.; Jones, L. M.; Kumar, G. D. K.; Conner, E. S.; Bayeh, L.; Chavarria, G. E.; Charlton-Sevcik, A. K.; Chen, S. E.; Chaplin, D. J.; Trawick, M. L.; Pinney, K. G. Synthesis and Biochemical Evaluation of Thiochromanone Thiosemicarbazone Analogues as Inhibitors of Cathepsin L. *ACS Med. Chem. Lett.* **2012**, *3* (6), 450–

453.

(53) Kishore Kumar, G. D.; Chavarria, G. E.; Charlton-Sevcik, A. K.; Arispe, W. M.; MacDonough, M. T.; Strecker, T. E.; Chen, S. E.; Siim, B. G.; Chaplin, D. J.; Trawick, M. L.; Pinney, K. G. Design, Synthesis, and Biological Evaluation of Potent Thiosemicarbazone Based Cathepsin L Inhibitors. *Bioorganic Med. Chem. Lett.* **2010**, *20* (4), 1415–1419.

(54) Kumar, G. D. K.; Chavarria, G. E.; Charlton-Sevcik, A. K.; Yoo, G. K.; Song, J.; Strecker, T. E.; Siim, B. G.; Chaplin, D. J.; Trawick, M. L.; Pinney, K. G. Functionalized Benzophenone, Thiophene, Pyridine, and Fluorene Thiosemicarbazone Derivatives as Inhibitors of Cathepsin L. *Bioorganic Med. Chem. Lett.* **2010**, *20* (22), 6610–6615.

(55) Copeland, R. A. *Enzymes: A Practical Introduction to Structure, Mechanism, and Data Analysis*, 2nd ed.; John Wiley and Sons Inc.: New York, 2000.

(56) Siles, R.; Chen, S.; Zhou, M.; Pinney, K. G.; Trawick, M. L. Design, Synthesis, and Biochemical Evaluation of Novel Cruzain Inhibitors with Potential Application in the Treatment of Chagas' Disease. *Bioorg. Med. Chem. Lett.* **2006**, *16* (16), 4405–4409.

(57) Neitz, R. J.; Bryant, C.; Chen, S.; Gut, J.; Hugo Caselli, E.; Ponce, S.; Chowdhury, S.; Xu, H.; Arkin, M. R.; Ellman, J. A.; Renslo, A. R. Tetrafluorophenoxymethyl Ketone Cruzain Inhibitors with Improved Pharmacokinetic Properties as Therapeutic Leads for Chagas' Disease. *Bioorganic Med. Chem. Lett.* **2015**, *25* (21), 4834–4837.